# Wall heat transfer effects on Klebanoff modes and Tollmien-Schlichting waves in a compressible boundary layer

Pierre Ricco
*Department of Mechanical Engineering, King's College London, Strand, London, WC2R 2LS United Kingdom*

Duc-Luan Tran
*Ecole Centrale de Lille, Cité Scientifique, BP 48 - 59651 Villeneuve d'Ascq, France*

Ganda Ye
*Division of Engineering, King's College London, Strand, London, WC2R 2LS United Kingdom*
(Dated: March 26, 2009)

**Published as Pierre Ricco, Duc-Luan Tran, and Ganda Ye *Wall heat transfer effects on Klebanoff modes and TollmienSchlichting waves in a compressible boundary layer* Phys. Fluids 21, 024106 (2009).**

The influence of wall heat transfer on fluctuations generated by free-stream vortical disturbances in a compressible laminar boundary layer is investigated. These disturbances are thermal Klebanoff modes, namely low-frequency, streamwise-elongated laminar streaks of velocity and temperature, and oblique Tollmien-Schlichting waves, induced by a leading-edge adjustment receptivity mechanism. The flow is governed by the linearized unsteady boundary-region equations, which properly account for the non-parallel and spanwise-diffusion effects, and for the continuous forcing of the free-stream convected gusts.

Wall cooling stabilizes the laminar streaks when their spanwise wavelength is much larger than the boundary-layer thickness. For these conditions, the disturbances confine themselves in the outer edge layer further downstream, where the compressibility effects are marginal. Klebanoff modes for which the spanwise diffusion is comparable with the wall-normal diffusion possess an asymptotic solution similarly to the incompressible case, and are stabilized by wall heating. The unstable waves, which appear in high-Mach-number subsonic and supersonic conditions, are stabilized by wall cooling and destabilized by wall heating. Removing heat from the surface significantly shifts downstream the starting location of instability, while the streamwise wavelength and the growth rate are less affected by the wall heat flux. Perturbation methods, such as the WKBJ technique and the triple-deck theory, are used effectively to validate the numerical results and to explain the flow physics.

## I. INTRODUCTION

This paper concerns the effects of wall heat transfer on low-frequency disturbances, such as Klebanoff modes[1–4] and Tollmien-Schlichting waves (TS)[5,6], appearing in pre-transitional laminar boundary layers when vortical disturbances are present in the outer free-stream. We consider disturbances evolving in a flat-plate, compressible Blasius boundary layer where the Mach number $M = \mathcal{O}(1)$, indicating that the free-stream velocities are comparable with the free-stream speed of sound. Both subsonic and supersonic conditions are studied.

The Klebanoff modes, or laminar streaks, are low-frequency, streamwise-elongated boundary-layer fluctuations. Their streamwise length scale is much larger than the boundary-layer thickness, while their spanwise length scale is usually comparable with the wall-normal length scale. The amplitude of the streamwise velocity component of the disturbance is usually much higher than the other velocity components and it peaks in the middle of the boundary layer. As outlined in Leib, Wundrow & Goldstein[7] (LWG), who studied the Klebanoff modes by perturbation and numerical methods, these boundary-layer disturbances are driven by the direct, continuous action of free-stream vortical perturbations. In particular, the spanwise component of the outer disturbances is mainly responsible for their generation. It is believed[8–10] that the laminar streaks, when exceeding a threshold amplitude, become nonlinear and may be subject to instability. They may quickly lead the boundary layer to transition through the formation of turbulent spots, and eventually to the fully-developed turbulent regime. This scenario has been often referred to as bypass transition to turbulence[11,12] because the classical linear instability mechanism involving Tollmien-Schlichting waves may not be relevant.

Historically, the first laboratory observations of the laminar streaks (also known as "breathing modes") date back to the works by Dryden[13] and Taylor[14], who showed that, when a laminar boundary layer is subjected to a medium-to-high level of free-stream turbulence, low-frequency disturbances within the viscous region significantly amplify and distort the flow. Renewed interest arose with the experimental investigations by Klebanoff[1] and Arnal & Juillen[15] because the transition process was not initiated by the modal growth mechanism, i.e. the TS-wave growth predicted by stability theory was not detected when the free-stream turbulence level exceeded a certain level. Further relevant experimental campaigns include Fransson *et al.*[16] and Hernon *et al.*[17,18] (and references therein). The works on the theoretical modeling of the laminar streaks are also numerous, and include for example Goldstein, Leib & Cowley[19], Luchini[20], Andersson, Berggren & Henningson[21]. Direct numerical simulations have also been employed to study the bypass transition process involving the laminar streaks[22,23] (and references therein).

The recent work by Ricco & Wu[24] (RW) has shown that *thermal* Klebanoff modes may be generated when free-stream vortical disturbances interact with a compressible laminar boundary layer. Although only vortical disturbances were present in the outer inviscid flow, both vorticity and thermal fluctuations were observed within the boundary layer because of the velocity-temperature coupling caused by compressibility. It was also shown that the thermal Klebanoff modes can evolve into low-frequency, oblique TS waves and that this mechanism is only physically relevant when the Mach number exceeds about 0.8. These disturbances are thus likely to be significant in laminar boundary layers over turbine blades[25,26] and wings of high-speed aircrafts, in wind-tunnel laboratories, or in other flows where the pre-transitional layers possess strong compressibility properties and are disturbed by free-stream vorticity fluctuations.

In this paper, prompted by the importance of these ubiquitous disturbances in compressible flow systems, we investigate the effects of wall cooling and wall heating with the aim of controlling the laminar boundary layer and attenuate the growth of such perturbations. While it is well accepted that cooling stabilizes first-mode, compressible TS waves[5], the effect of wall heat transfer on the Klebanoff modes is still unknown. The present work is based on the theoretical framework of RW, i.e. the linearized, compressible, unsteady boundary-region equations, which describe the motion of the thermal Klebanoff modes. This differential system is inhomogeneous with respect to the outer boundary conditions, in that the boundary-layer disturbances are continuously forced by the

free-stream vortical fluctuations. For further details on the formulation on the boundary-region equations, the reader should refer to LWG. We also resort to perturbation methods, such the WKBJ technique and the triple-deck theory, in order to validate the numerical calculations and explain the flow physics.

The paper is organized as follows. The asymptotic structure of the flow domain and the governing equations with the relative initial and boundary conditions are presented in §II. The results are contained in §III, which is divided into four subsections. In §III A, the effect of different wall boundary conditions on the thermal fluctuations is studied, while the influence of the wall heat flux on the Klebanoff modes is investigated in §III B and §III C, and on the oblique Tollmien-Schlichting waves in §III D. Section §IV briefly outlines the results and presents a diagram which summarizes the flow regimes and the effects of the wall heat transfer on the disturbances.

## II. MATHEMATICAL FORMULATION

The mathematical framework and the numerical procedures for the solution of the boundary-region problem are presented in this section. Further details are found in LWG and RW.

### A. Scaling and asymptotic structure of flow domain

We consider a flow of air of uniform velocity $U_\infty$ and temperature $T_\infty$ past an infinitely-thin flat plate. The Mach number is defined as $M \equiv U_\infty/c_\infty = \mathcal{O}(1)$, where $c_\infty = \sqrt{\gamma \mathcal{R} T_\infty}$ is the speed of sound in the free-stream, $\gamma = 1.4$ is the ratio of the specific heats and $\mathcal{R} = 287.05$ Nmkg$^{-1}$K$^{-1}$ is the universal gas constant. Both subsonic ($M < 1$) and supersonic conditions ($M > 1$) are considered. A wall heat flux is imposed, so that wall cooling and wall heating conditions can be studied. Superimposed on $U_\infty$ are small, homogeneous, statistically-stationary vortical fluctuations. These perturbations are of the convected gust type, i.e. they advect at a velocity $U_\infty$.

The flow is described by a Cartesian coordinate system, where $x^*, y^*$ and $z^*$ define the streamwise, wall-normal and spanwise directions, respectively. The streamwise coordinate is scaled by the gust streamwise wavenumber $k_x^* = 2\pi/\lambda_x^*$, i.e. $\overline{x} = 2\pi x^*/\lambda_x^* = \mathcal{O}(1)$, where $\lambda_x^*$ is the streamwise wavelength. The wall-normal coordinate is non-dimensionalized by $\delta^*$, a measure of the thickness of the mean laminar boundary layer, so that the similarity variable $\eta = y^*/\delta^* = \mathcal{O}(1)$ is defined. A precise definition of $\eta$ is given later in equation (2). The spanwise wavelength $\lambda_z^*$ is used to scale the spanwise coordinate, i.e. $z = z^*/\lambda_z^* = \mathcal{O}(1)$. The velocities and the temperature are scaled by $U_\infty$ and $T_\infty$. The pressure is normalized by $\rho_\infty^* U_\infty^2$ (where $\rho_\infty^*$ is the constant free-stream density). The density $\rho^*$, the thermal conductivity $\mathcal{K}^*$, and the dynamic viscosity $\mu^*$ are scaled by their respective free-stream values. The symbol $^*$ indicates a dimensional quantity.

Mathematically, the free-stream vorticity fluctuations can be represented as a superposition of sinusoidal disturbances:

$$\mathbf{u}^* = U_\infty + \epsilon \hat{\mathbf{u}}^{\infty *} E + c.c., \quad E = \mathrm{e}^{i(\mathbf{k}^* \cdot \mathbf{x}^* - k_x^* t^*)},$$

where $\hat{\mathbf{u}}^{\infty *} = \{\hat{u}_x^{\infty *}, \hat{u}_y^{\infty *}, \hat{u}_z^{\infty *}\}$, $\hat{u}_{x,y,z}^{\infty} = \mathcal{O}(1)$, and $\mathbf{k}^* = \{k_x^*, k_y^*, k_z^*\}$ are real vectors, $\epsilon$ is a measure of the turbulence intensity and *c.c.* denotes the complex conjugate. It follows from the continuity equation that

$$\mathbf{k}^* \cdot \hat{\mathbf{u}}^{\infty *} = 0. \tag{1}$$

We focus on low-frequency, streamwise-elongated disturbances with $\lambda_z^*/\lambda_x^*, \lambda_y^*/\lambda_x^* \ll 1$. These are the fluctuations that penetrate the most into the boundary layer to form the laminar streaks, as emerges from numerous experimental works[1–4]. In order to simplify the analysis, we consider gusts with equal wall-normal and spanwise wavelengths, so that $\lambda_y^* = \lambda_z^*$. The flow is studied at a downstream location

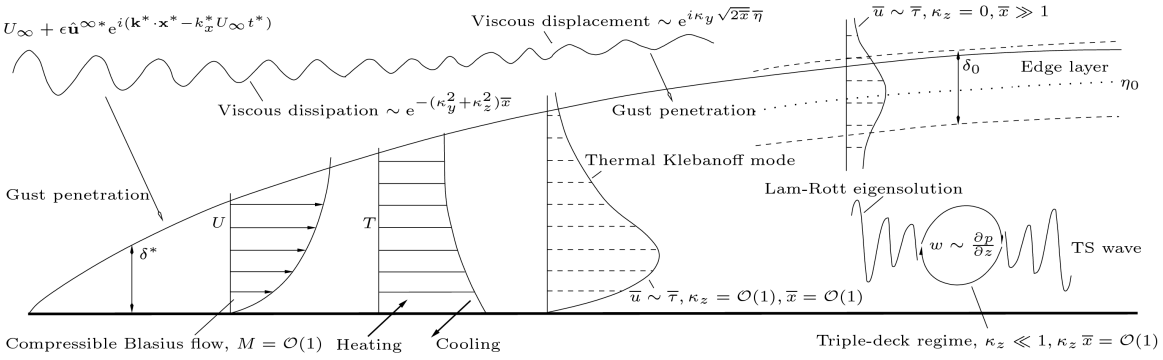


FIG. 1: Schematic of the physical domain.

where $\overline{x} = \mathcal{O}(1)$, namely at a distance from the leading edge which is comparable with the streamwise wavelength of the gust. Guided by experimental evidence[3,4], which reveals that the spanwise length scale of the laminar streaks is comparable with the mean boundary-layer thickness, we assume that $\lambda_z^* = \mathcal{O}(\delta^*)$. Among other things, this implies that the spanwise viscous diffusion is of the same order of the wall-normal viscous diffusion. The boundary-layer disturbances are therefore governed by the unsteady boundary-region equations[27], which are a rigorous asymptotic limit of the Navier-Stokes equations for low-frequency disturbances. In this limit, the streamwise pressure gradient and the streamwise viscous diffusion terms may be neglected at leading order. More precisely, these terms are $\mathcal{O}[(\lambda_z^*/\lambda_x^*)^2]$ smaller than the wall-normal and spanwise diffusion terms. The asymptotic analysis by LWG shows that the disparity between the spanwise and the streamwise length scales allows $\mathcal{O}(\epsilon)$ fluctuations in the free-stream to generate $\mathcal{O}(\epsilon k_z^*/k_x^*)$ streamwise velocity disturbances within the boundary layer. We consider small-amplitude disturbances, so that the condition for linearization within the boundary-layer is $\epsilon k_z^*/k_x^* \ll 1$. A schematic of the physical domain is presented in figure 1.

### B. Governing equations

The equations of motion for the mean flow and for the disturbances are introduced in this section. The wall-normal similarity variable $\eta$ may be written as

$$\eta \equiv \left(\frac{U_\infty}{2\nu_\infty^* x^*}\right)^{1/2} \int_0^{y^*} \frac{\rho^*}{\rho_\infty^*} \mathrm{d}\breve{y}^*, \tag{2}$$

where $\nu_\infty^*$ is the free-stream kinematic viscosity. The mean flow solution is

$$U = F'(\eta), \quad V = \left(\frac{\nu_\infty^*}{2x^* U_\infty}\right)^{1/2} (\eta_c T F' - T F), \quad T = T(\eta),$$

where $U$ and $V$ are the mean streamwise and wall-normal velocity components, and $T$ is the mean temperature. The prime denotes differentiation with respect to $\eta$, and $\eta_c \equiv (1/T)\int_0^\eta T(\breve{\eta})\mathrm{d}\breve{\eta}$. The $x$-momentum and energy equations are written as[28]

$$[(\mu/T)F'']' + FF'' = 0, \tag{3}$$

$$\mathrm{Pr}^{-1}\,[(\mu/T)T']' + FT' + (\gamma-1)M^2(\mu/T)F''^2 = 0. \tag{4}$$

where Pr=0.7 is the Prandtl number. The boundary conditions are

$$F(0) = F'(0) = 0, \quad T'(0) = T_{dw}; \quad F' \to 1, \; T \to 1 \;\; \text{as} \;\; \eta \to \infty.$$

The first two expressions indicate the no-slip condition at the wall, i.e. $U = V = 0$ at $y = 0$. The condition on the temperature gradient expresses the heat flux at the wall. Cooling occurs for $T_{dw} > 0$ and heating for $T_{dw} < 0$. $T_{dw}$ varies between -0.2 and 0.2 in the present study. This thermal condition at the wall corresponds to the following $x^*$-dependent local wall heat flux

$$Q_w^* = -\mathcal{K}^*(0)\frac{\partial T^*}{\partial y^*}\bigg|_{x^*=0} = -\frac{\mathcal{K}^*(0)}{T(0)}\left(\frac{U_\infty}{2\nu_\infty^* x^*}\right)^{1/2} T_{dw}.$$

Note that this kind of heat flux is considered in order to express the mean temperature profile in terms of the similarity variable $\eta$ and avoid the dependence of the mean flow on the streamwise coordinate in the numerical calculations. The conditions as $\eta \to \infty$ indicate that the mean streamwise velocity and the mean temperature in the boundary layer match the free-stream mean velocity and mean temperature, respectively. It is also assumed that the dynamic viscosity and the thermal conductivity depend on the mean temperature as follows[28]

$$\mu = \mathcal{K} = T^{0.76},$$

which is acceptable for the Mach number range of interest ($M \leq 3$)[29].

For a single Fourier component of the disturbance, the fluctuations in the boundary layer are

$$\{u, v, w, \tau, p\} = \epsilon \left\{ \overline{u}_0(\overline{x}, \eta), \left(\frac{2\nu_\infty^* x^*}{(\lambda_x^*)^2 U_\infty}\right)^{1/2} \overline{v}_0(\overline{x}, \eta), \overline{w}_0(\overline{x}, \eta), \overline{\tau}_0(\overline{x}, \eta), \overline{p}_0(\overline{x}, \eta) \right\} E \; + \; c.c.,$$

where $\tau$ and $p$ indicate the temperature and the pressure fluctuations. Following Gulyaev *et al.*[30] and LWG, the solution is expressed as a sum of a two-dimensional part and a three-dimensional part, namely

$$\begin{aligned}
&\{\overline{u}_0, \overline{v}_0, \overline{\tau}_0\} = \left(\hat{u}_x^\infty + \tfrac{i}{((k_z^*/k_x^*)^2+1)^{1/2}}\hat{u}_y^\infty\right)\{\overline{u}^{(0)}, \overline{v}^{(0)}, \overline{\tau}^{(0)}\} \\
&+\tfrac{ik_z^*}{k_x^*}\left(\hat{u}_z^\infty + \tfrac{i}{((k_x^*/k_z^*)^2+1)^{1/2}}\hat{u}_y^\infty\right)\{\overline{u}, \overline{v}, \overline{\tau}\}, \\
&\overline{w}_0 = \left(\hat{u}_z^\infty + \tfrac{i}{((k_x^*/k_z^*)^2+1)^{1/2}}\hat{u}_y^\infty\right)\overline{w}, \\
&\overline{p}_0 = \tfrac{k_x^*\nu_\infty^*}{U_\infty}\left(\hat{u}_x^\infty + \tfrac{i}{((k_x^*/k_z^*)^2+1)^{1/2}}\hat{u}_y^\infty\right)\overline{p}^{(0)} + i\kappa_z\left(\tfrac{k_x^*\nu_\infty^*}{U_\infty}\right)^{1/2}\left(\hat{u}_z^\infty + \tfrac{i}{((k_x^*/k_z^*)^2+1)^{1/2}}\hat{u}_y^\infty\right)\overline{p}.
\end{aligned} \tag{5}$$

The two-dimensional part is smaller than the three-dimensional part by a factor $k_x^*/k_z^* \ll 1$, and hence will not be considered any further. The compressible boundary-region equations read:

$$\frac{\partial \overline{u}}{\partial \overline{x}} + \frac{\eta_c}{2\overline{x}}\left(\frac{T'}{T}\overline{u} - \frac{\partial \overline{u}}{\partial \eta}\right) - \frac{T'}{T^2}\overline{v} + \frac{1}{T}\frac{\partial \overline{v}}{\partial \eta} + \overline{w} + \left(\frac{i}{T} - \frac{FT'}{2\overline{x}T^2}\right)\overline{\tau} - \frac{F'}{T}\frac{\partial \overline{\tau}}{\partial \overline{x}} + \frac{F}{2\overline{x}T}\frac{\partial \overline{\tau}}{\partial \eta} = 0, \tag{6}$$

$$\begin{aligned}
&\left(-i - \frac{\eta_c F''}{2\overline{x}} + \mu\kappa_z^2 T\right)\overline{u} + F'\frac{\partial \overline{u}}{\partial \overline{x}} - \frac{1}{2\overline{x}}\left(F + \frac{\mu' T'}{T} - \frac{\mu T'}{T^2}\right)\frac{\partial \overline{u}}{\partial \eta} - \frac{\mu}{2\overline{x}T}\frac{\partial^2 \overline{u}}{\partial \eta^2} + \frac{F''}{T}\overline{v} \\
&+ \left(\frac{FF'' - \mu'' T' F'' - \mu' F'''}{2\overline{x}T} + \frac{\mu' F'' T'}{2\overline{x}T^2}\right)\overline{\tau} - \frac{\mu' F''}{2\overline{x}T}\frac{\partial \overline{\tau}}{\partial \eta} = 0,
\end{aligned} \tag{7}$$

$$\frac{1}{4\overline{x}^2}\left[FT+\eta_c(FT'-TF')-\eta_c^2F''T\right]\overline{u}+\frac{\mu'T'}{3\overline{x}}\frac{\partial\overline{u}}{\partial\overline{x}}-\frac{\mu}{6\overline{x}}\frac{\partial^2\overline{u}}{\partial\overline{x}\partial\eta}$$

$$+\frac{1}{12\overline{x}^2}\left[\mu+\eta_cT\left(\frac{\mu}{T}\right)'\right]\frac{\partial\overline{u}}{\partial\eta}+\frac{\eta_c\mu}{12\overline{x}^2}\frac{\partial^2\overline{u}}{\partial\eta^2}$$

$$+\left(-i+\mu\kappa_z^2T+\frac{F'}{2\overline{x}}+\frac{\eta_cF''}{2\overline{x}}-\frac{FT'}{2\overline{x}T}\right)\overline{v}+F'\frac{\partial\overline{v}}{\partial\overline{x}}$$

$$-\frac{1}{\overline{x}}\left(\frac{F}{2}+\frac{2\mu'T'}{3T}-\frac{2\mu T'}{3T^2}\right)\frac{\partial\overline{v}}{\partial\eta}-\frac{2\mu}{3\overline{x}T}\frac{\partial^2\overline{v}}{\partial\eta^2}+\frac{\mu'T'}{3\overline{x}}\overline{w}-\frac{\mu}{6\overline{x}}\frac{\partial\overline{w}}{\partial\eta}+\frac{1}{2\overline{x}}\frac{\partial\overline{p}}{\partial\eta}$$

$$+\frac{1}{4\overline{x}^2}\left\{\eta_c\left[(FF')'-T\left(\frac{\mu'F''}{T}\right)'\right]-FF'-\frac{F^2T'}{T}-\mu'F''+\frac{4}{3}\left(\frac{\mu'T'F}{T}\right)'\right\}\overline{\tau}$$

$$-\frac{\mu'F''}{2\overline{x}}\frac{\partial\overline{\tau}}{\partial\overline{x}}-\left(\frac{\eta_c\mu'F''}{4\overline{x}^2}-\frac{\mu'T'F}{3\overline{x}^2T}\right)\frac{\partial\overline{\tau}}{\partial\eta}=0, \tag{8}$$

$$-\frac{\eta_c\mu'T'T\kappa_z^2}{2\overline{x}}\overline{u}+\frac{\mu T\kappa_z^2}{3}\frac{\partial\overline{u}}{\partial\overline{x}}-\frac{\eta_c\mu T\kappa_z^2}{6\overline{x}}\frac{\partial\overline{u}}{\partial\eta}+\mu'T'\kappa_z^2\overline{v}+\frac{\mu\kappa_z^2}{3}\frac{\partial\overline{v}}{\partial\eta}-\left(i-\frac{4\mu T\kappa_z^2}{3}\right)\overline{w}$$

$$+F'\frac{\partial\overline{w}}{\partial\overline{x}}-\frac{1}{2\overline{x}}\left(F+\frac{\mu'T'}{T}-\frac{\mu T'}{T^2}\right)\frac{\partial\overline{w}}{\partial\eta}-\frac{\mu}{2\overline{x}T}\frac{\partial^2\overline{w}}{\partial\eta^2}+\frac{\mu'FT'\kappa_z^2}{3\overline{x}}\overline{\tau}-\kappa_z^2T\overline{p}=0, \tag{9}$$

$$-\frac{\eta_cT'}{2\overline{x}}\overline{u}-\frac{M^2(\gamma-1)\mu F''}{\overline{x}T}\frac{\partial\overline{u}}{\partial\eta}+\frac{T'}{T}\overline{v}$$

$$+\left[-i+\frac{FT'}{2\overline{x}T}-\frac{1}{2\mathrm{Pr}\overline{x}}\left(\frac{\mu'T'}{T}\right)'-\frac{M^2(\gamma-1)\mu'F''^2}{2\overline{x}T}+\frac{\mu\kappa_z^2T}{\mathrm{Pr}}\right]\overline{\tau}$$

$$+F'\frac{\partial\overline{\tau}}{\partial\overline{x}}-\frac{1}{2\overline{x}}\left(F+\frac{2\mu'T'}{\mathrm{Pr}T}-\frac{\mu T'}{\mathrm{Pr}T^2}\right)\frac{\partial\overline{\tau}}{\partial\eta}-\frac{\mu}{2\mathrm{Pr}\overline{x}T}\frac{\partial^2\overline{\tau}}{\partial\eta^2}=0, \tag{10}$$

where

$$\kappa_z\equiv\sqrt{\frac{2\pi\nu_\infty^*\lambda_x^*}{U_\infty}}\frac{1}{\lambda_z^*}=\mathcal{O}(1),$$

and the prime on $\mu$ indicates differentiation with respect to $T$. The incompressible boundary-region equations (LWG) can be recovered by setting $M=0$[51], $T=1$, $\mu=1$, $\overline{\tau}=0$ and by using the continuity equation (6). At $\overline{x}=\mathcal{O}(1)$, $\kappa_z=\mathcal{O}(\delta^*/\lambda_z^*)$, so that the spanwise viscous diffusion is comparable with the wall-normal viscous diffusion. When $\kappa_z\ll1$, the spanwise diffusion effects are negligible and the boundary-region equations simplify to the boundary-layer equations (see equations (4.5)-(4.6) at page 176 in LWG for the incompressible case). The wall boundary conditions for the

velocity components are $\overline{u} = \overline{v} = \overline{w} = 0$ at $\eta = 0$, which express the no-slip condition. Two different wall thermal boundary conditions are considered:

$$\overline{\tau} = 0 \ \text{ or } \ \frac{\partial \overline{\tau}}{\partial \eta} = 0 \ \text{ at } \ \eta = 0. \tag{11}$$

They are studied in detail in §III A. As the free-stream is approached, the boundary-layer fluctuations match with the convective gust disturbances and the following outer boundary conditions are found

$$\overline{u} \to 0, \overline{\tau} \to 0, \mathcal{L}(\boldsymbol{\chi}) \to \upsilon \cdot \boldsymbol{\xi} \ \text{ as } \ \eta \to \infty,$$

where

$$\begin{aligned} &\mathcal{L} = \partial/\partial\eta + |\kappa_z|(2\overline{x})^{1/2}, \\ &\boldsymbol{\chi} = \{\overline{v}, \overline{w}, \overline{p}\}, \\ &\boldsymbol{\xi} = \{-1, i\kappa_y(2\overline{x})^{1/2}, 0\}, \\ &\upsilon = \mathrm{e}^{i\left(\overline{x}+\kappa_y(2\overline{x})^{1/2}\overline{\eta}\right)}\mathrm{e}^{-\left(\kappa_z^2+\kappa_y^2\right)\overline{x}}, \end{aligned}$$

$\kappa_y \equiv \sqrt{(2\pi\nu_\infty^* \lambda_x^*)/U_\infty}/\lambda_y^* = \mathcal{O}(1)$ and $\overline{\eta} \equiv \eta - \beta_c$ (see the Appendix for the definition and properties of $\beta_c$, and LWG and RW for the derivation of the outer boundary conditions). Note that the wall-normal wavenumber $\kappa_y$ only appears in the outer boundary conditions and not in the boundary-region equations. This is because the wall-normal length scale of the disturbance in the outer flow is $\lambda_y^*$, while within the boundary layer the characteristic length scale of the fluctuations is the boundary-layer thickness itself, so that $\lambda_y^*$ becomes irrelevant there. The appropriate initial conditions for the boundary-region equations are found by seeking the following power series solution for $\eta = \mathcal{O}(1)$ and $\overline{x} \ll \mathcal{O}(1)$

$$\{\overline{u}, \overline{v}, \overline{w}, \overline{\tau}, \overline{p}\} = \sum_{n=0}^{\infty} (2\overline{x})^{n/2} \left\{2\overline{x}U_n(\eta), V_n(\eta), W_n(\eta), 2\overline{x}T_n(\eta), P_n(\eta)/(2\overline{x})^{1/2}\right\}. \tag{12}$$

Substituting (12) into the boundary-region equations (6)-(10) and collecting like powers of $\overline{x}$, a system of ordinary differential equations is obtained. The reader is referred to LWG and RW for details on the initial conditions.

The mean-flow equations (3) and (4) are solved by a second-order, implicit finite-difference scheme, and nonlinearity is treated by Newton-Raphson iteration[28]. The boundary-region equations are parabolic in the $\overline{x}$ direction and elliptic in the $z$ direction, so that they are solved by marching downstream by applying the initial conditions, the outer boundary conditions, and the conditions at the wall. A second-order, implicit finite-difference scheme which is central in $\eta$ and backward in $\overline{x}$ is used. The pressure terms are computed on a grid staggered in the $\eta$ direction with respect to the grid for the velocity components to eliminate the pressure decoupling phenomenon, which occurs if the two grids coincide. The linear system is solved by a standard block-elimination algorithm. A uniform grid with a typical mesh size of $\Delta\eta = 0.05$ is employed and the domain extends to $\eta = 30$. The downstream integration is started at $\overline{x} = 10^{-3}$ and the integration step is $\Delta\overline{x} = 10^{-4}$. The interested reader should refer to Ricco[31] for more details on the numerical procedures.

## III. RESULTS

The effects of the wall heat flux on the velocity, temperature and mass-flux fluctuations are presented. The mass-flux disturbance $|\overline{\rho u}|$, a quantity usually measured in experiments of compressible flows[32], is defined as

$$|\overline{\rho u}| = |(\rho + \overline{\rho})(U + \overline{u}) - \rho U| \approx |\rho\overline{u} + \overline{\rho}U| = \left|\frac{\overline{u}}{T} - \frac{U\overline{\tau}}{T^2}\right|.$$

We assume that the variation of the Mach number $M$ is only due to the change of $U_\infty$, while $T_\infty$ is constant, and that the modulus of the gust vector remains equal to unity, i.e. $[(\hat{u}_x^\infty)^2 + (\hat{u}_y^\infty)^2 + (\hat{u}_z^\infty)^2]^{1/2} = 1$. We further consider that, when $M$ varies, $k_x^*$ is kept constant, $\hat{u}_x^\infty = 1$, and $\kappa_z = \kappa_y$, so that the properties of the gust are fully specified by use of equation (1). In the following subsections, the effect of the wall boundary conditions on the temperature fluctuations $\overline{\tau}$ is studied in §III A, the influence of the wall heat flux on the Klebanoff modes is investigated in §III B for $\kappa_z = 0$, in §III C for $\kappa_z = \mathcal{O}(1)$, and on the TS waves in §III D for $\kappa_z \ll 1$. Unless otherwise stated, a dash-dot line indicates wall-cooling conditions, a dashed line denotes wall-heating conditions, and a solid line refers to adiabatic-wall conditions in the following figures.

### A. Effect of wall boundary conditions on temperature disturbances

As mentioned in §II B, the wall boundary condition on the thermal disturbance may be specified on the temperature fluctuation ($\overline{\tau}(0) = 0$) or on its gradient ($\partial\overline{\tau}/\partial\eta|_{\eta=0} = 0$). The Dirichlet boundary condition is usually employed in stability studies of compressible boundary layers with high frequency disturbances[33], while the Neumann boundary condition is often adopted for stationary, or nearly stationary flows, such as cross-flow disturbances[34]. RW have adopted the Dirichlet boundary condition in their study of thermal Klebanoff modes and TS waves. Dunn & Lin[35] have shown that the wall boundary condition on the temperature fluctuation may depend on the surface material, its thickness, the method of cooling/heating and the frequency of the disturbances. It is therefore interesting to study the effect of both boundary conditions on the development of the thermal Klebanoff modes. The maximum (along $\eta$) of the velocity and temperature fluctuations for both wall conditions at $M$=2 and $T_{dw} = 0.2$ is shown in figure 2 for $\kappa_z = 0$ and in figure 3 for $\kappa_z = 1$. The profiles differ slightly when $\overline{x} = \mathcal{O}(1)$, but the effect vanishes further downstream. When $\kappa_z = 0$, the trends of maximum velocity and temperature coincide for $\overline{x} > 6$ (see figure 2). The influence of the temperature wall boundary condition is irrelevant for $\overline{x} > 2$ when $\kappa_z = 1$, as shown in figure 3. When $\kappa_z = 0$, this behavior can be predicted by an asymptotic study in the limit $\overline{x} \to \infty$. The following is an extension of LWG's analysis to the compressible regime. For $\overline{x} \gg 1$ and $\eta = \mathcal{O}(1)$, the solution takes the WKBJ form

$$\{\overline{u}, \overline{v}, \overline{w}, \overline{\tau}\} = \left\{\overline{U}(\eta, \overline{x}), \frac{\overline{V}(\eta, \overline{x})}{(2\overline{x})^{1/2}}, \overline{W}(\eta, \overline{x}), \overline{T}(\eta, \overline{x})\right\} \mathrm{e}^{i\overline{x} - (2\overline{x})^{1/2}\Theta(\eta)}. \tag{13}$$

The boundary conditions (11) become

$$\overline{T} = 0 \quad \text{or} \quad \overline{T}' - (2\overline{x})^{1/2}\Theta'\overline{T} = 0 \quad \text{at} \quad \eta = 0, \tag{14}$$

where the prime indicates partial derivative with respect to $\eta$. Inserting the disturbances (13) into the boundary-region equations (7) and (10) and retaining the leading-order terms, one arrives at:

$$\left[F'\Theta - \left(F + \frac{\mu' T'}{T} - \frac{\mu T'}{T^2}\right)\Theta' - \frac{\mu\Theta''}{T}\right]\overline{U} - \frac{2\mu\Theta'}{T}\overline{U}' - \frac{F''}{T}\overline{V} + \frac{\mu' F''\Theta'}{T}\overline{T} = 0, \tag{15}$$

$$\frac{2M^2(\gamma-1)\mu F''\Theta'}{T}\overline{U}' + \frac{T'}{T}\overline{V} + \left[-F'\Theta + \left(F + \frac{2\mu' T'}{\mathrm{Pr}T} - \frac{\mu T'}{\mathrm{Pr}T^2}\right)\Theta' + \frac{\mu\Theta''}{\mathrm{Pr}T}\right]\overline{T} + \frac{2\mu\Theta'}{\mathrm{Pr}T}\overline{T}' = 0, \tag{16}$$

and

$$\Theta(\eta) = \mathrm{e}^{-i\pi/4}\int_\eta^\infty \left[(1 - F')\frac{T}{\mu}\right]^{1/2} \mathrm{d}\breve{\eta},$$

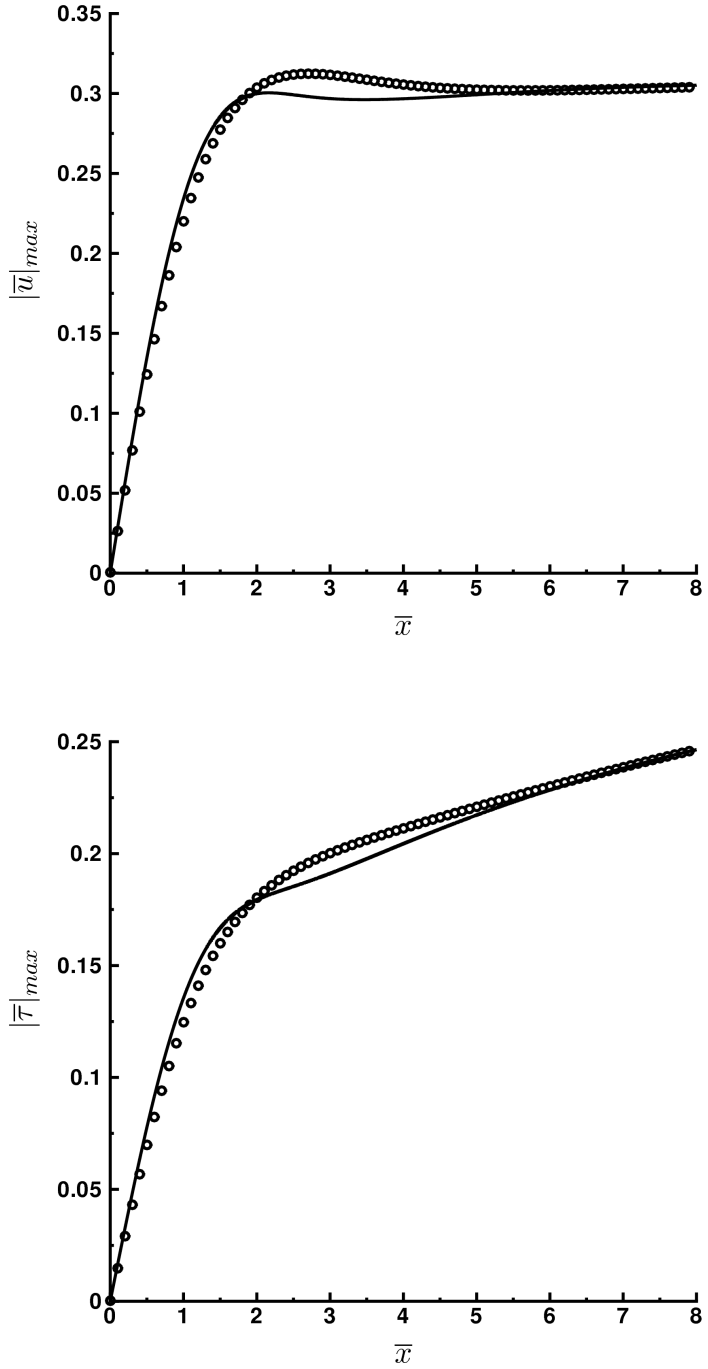


FIG. 2: Maximum (across $\eta$) of the streamwise velocity (top) and temperature fluctuation (bottom) for $M$=2, $T_{dw} = 0.2$ and $\kappa_z = 0$. In this figure and in figure 3, the lines represent cases with $\overline{\tau}(0) = 0$ and the symbols denote cases with $\partial\overline{\tau}/\partial\eta|_{\eta=0} = 0$.

which is found by integration of the lower-order term obtained by substitution of the spanwise velocity component of (13) into equation (9). By setting $\eta = 0$ in equation (15), it follows that

$$\overline{U}'(0) = \frac{\mu'(0)F''(0)\Theta'(0)}{2\mu(0)\Theta'(0)}\overline{T}(0).$$

This expression is substituted into equation (16) to find

$$A\,\overline{T}(0) \,+\, B\,\overline{T}'(0) = 0, \tag{17}$$

where $A$ and $B$ are $\mathcal{O}(1)$-constants. From equations (14) and (17), it follows that the two temperature boundary conditions, $\overline{\tau}(0) = 0$ and $\partial\overline{\tau}/\partial\eta|_{\eta=0} = 0$, may be used indifferently at large $\overline{x}$. The most general case where a mixed boundary condition such as (17) is imposed also leads to the same result when $\overline{x} \gg 1$. The Dirichlet boundary condition was used in the following analysis.

### B. Klebanoff modes for $\kappa_z \ll 1$

In this section, we study the effect of wall heat flux on the boundary-layer disturbances with asymptotically small values of $\kappa_z$. As $\kappa_z$ is of the same order of the ratio between the boundary-layer thickness $\delta^*$ and the spanwise wavelength $\lambda_z^*$ when $\overline{x} = \mathcal{O}(1)$, the spanwise diffusion is negligible in the present case. It follows that the amplifying effects of the free-stream forcing and of the mean flow shear within the boundary layer balance the dissipative action of the wall-normal diffusion, so that the Klebanoff modes persist indefinitely within the boundary layer, as shown in figure 2 at page 178 in LWG for the incompressible case. The other important feature is that, when $\overline{x} \gg 1$, the disturbances confine themselves in the so-called edge layer, which is located in the proximity of the free-stream, while they are vanishingly small in the core of the boundary layer. The first idea of boundary layer disturbances moving toward the outer flow was put forward by Brown & Stewartson[36], who studied the homogeneous unsteady boundary layer disturbances by asymptotic analysis. The concept of the edge layer was later resumed by Gulyaev *et al.*[30] and by LWG to study the Klebanoff modes. Their analysis is extended here to the compressible regime in order to validate the numerical results.

The downstream evolution of the compressible boundary-layer fluctuations is qualitatively similar to the incompressible case studied by LWG. Figure 4 shows that for adiabatic-wall conditions the streamwise velocity and the temperature fluctuations are both amplified by the viscous heating, which occurs when $M = \mathcal{O}(1)$. The effect is more intense on the thermal disturbances. Note that, as the Mach number variation is only caused by a change of $U_\infty$, and $\hat{u}^\infty_{x,y,z}$ and $\lambda_x^*$ are kept constant, the effect of $M$ on $\overline{u}_0$ and $\overline{\tau}_0$ may be studied through $\overline{u}$ and $\overline{\tau}$ because the coefficient of proportionality between these quantities remains constant (see equation (5)). The destabilizing effect of $M$ has also been observed in other transiently growing disturbances, such as the algebraically-growing, streamwise-independent fluctuations studied by Hanifi, Schmid & Henningson[37] and Hanifi & Henningson[38].

As expected from the above results, wall heating has the same effect of an increment of $M$, i.e. it destabilizes the streamwise velocity and the mass-flux fluctuations. Wall cooling is instead stabilizing. This occurs for both subsonic and supersonic conditions, as shown in figure 5 for the downstream evolution of the maximum (along $\eta$) of the fluctuations. Figure 6 presents the influence of the wall heat flux on the profiles of the disturbances for $M = 2$. The thermal fluctuations are affected the most, while the distribution of the spanwise velocity component is almost unvaried. The circles in the middle graph show the temperature profile for wall cooling when the Neumann boundary condition is employed (see also figure 11). The trend agrees with the one obtained via the Dirichlet wall boundary condition in the core of the boundary layer, while the curve differ for $\eta < 1.2$. The effect is negligible for wall heating and on the velocity components.

While the quantities $\overline{u}$, $\overline{w}$ and $\overline{\rho u}$ decay monotonically as $T_{dw}$ increases, the thermal fluctuations $\overline{\tau}$ are destabilized by heating for any $M$ and stabilized by cooling for supersonic conditions, but cooling

may have either effects in subsonic conditions. In figure 5, $|\overline{\tau}|_{max}$ increases with either cooling or heating at $M = 0.75$, and is destabilized by heating and stabilized by cooling at $M = 2$. This behavior may be explained as follows. In figure 7, the temperature fluctuation $|\overline{\tau}|_{max}$ at $\overline{x} = 1$ is shown as a function of $T_{dw}$ for different Mach numbers. When $M = 0$, $|\overline{\tau}|$ are null for adiabatic-wall conditions because the flow is incompressible. They increase as either cooling or heating is applied because the flow becomes compressible. A mean temperature gradient is generated by the wall heat flux, which produces a coupling between the temperature and velocity fluctuations. The fluctuations $|\overline{\tau}|_{max}$ respond linearly to a change of $T_{dw}$ and the trend is symmetric about $T_{dw} = 0$. As the Mach number increases, the same trend is found, but it is shifted to higher $T_{dw}$ values, so that cooling may intensify or attenuate the fluctuations. When $M > 1.5$, the trend crosses the abscissa for $T_{dw} > 0.2$, which corresponds to a too high value of wall cooling and does not represent physically realizable conditions. Therefore, beyond this Mach number, $|\overline{\tau}|_{max}$ always decays as $T_{dw}$ increases.

Figure 8 shows the $\eta$ location of the maximum of the streamwise velocity fluctuations, $|\overline{u}|_{max}$, as a function of $\overline{x}$ for different compressible conditions. The fluctuations concentrate in the core of the boundary layer when $\overline{x} = \mathcal{O}(1)$ and eventually move upward toward the free-stream as the flow evolves downstream. They concentrate in the edge layer at $\eta \approx 3$ for large $\overline{x}$. Removing heat from the surface shifts the fluctuations upward and the effect is more intense in subsonic conditions.

The wall heat transfer effect can be predicted by an asymptotic analysis on the spanwise velocity fluctuations $\overline{w}$ in the limit $\overline{x} \gg 1$. The estimates by the asymptotic analysis at large $\overline{x}$ may be considered valid at any $\overline{x}$ because the numerical trends for different wall heat transfer conditions do not cross as $\overline{x}$ varies. As discussed previously, in the large-$\overline{x}$ limit, the fluctuations decay rapidly in the core of the boundary layer and move upward toward the edge layer. Following Gulyaev *et al.*[30] and LWG, the equations for the compressible edge layer are derived and solved analytically for the spanwise velocity component. The edge layer is centered at $\eta_0$, with $\eta_0$ determined by

$$\frac{2\overline{x}A_F}{\eta_0^3 \mathrm{e}^{\eta_0^2/2}} = \mathcal{O}(1), \tag{18}$$

where $A_F$ depends on the Mach number and on the wall heat flux. It is studied in detail in the Appendix. A local transverse coordinate is introduced

$$\hat{\eta} \equiv \frac{\overline{\eta} - \eta_0}{\delta_0}, \tag{19}$$

where $\delta_0(\overline{x})$ is the edge-layer thickness. By balancing the inertia and viscous terms in the $z$-momentum equation (9) with $\Theta = \mathcal{O}((2\overline{x})^{-1/2})$, one finds

$$\delta_0 \eta_0 = \mathcal{O}(1). \tag{20}$$

The edge layer is depicted in the top-right corner of figure 1. The solution for the disturbance may be written as

$$\{\overline{u}, \overline{v}, \overline{w}, \overline{\tau}\} = \{\overline{u}_e, \delta_0 \overline{v}_e, \overline{w}_e, \overline{\tau}_e\} \mathrm{e}^{i\overline{x}}. \tag{21}$$

By substituting (21) into the boundary-layer equations and by using (19) and (20), one obtains the following compressible edge-layer equations:

$$i\overline{u}_e + \frac{\mathrm{d}\overline{v}_e}{\mathrm{d}\hat{\eta}} + \overline{w}_e + i\overline{\tau}_e \mathrm{e}^{-\hat{\eta}} + \frac{\mathrm{d}\overline{\tau}_e}{\mathrm{d}\hat{\eta}} = 0,$$

$$(i\overline{u}_e - \overline{v}_e)\mathrm{e}^{-\hat{\eta}} + \frac{\mathrm{d}\overline{u}_e}{\mathrm{d}\hat{\eta}} + \frac{\mathrm{d}^2\overline{u}_e}{\mathrm{d}\hat{\eta}^2} = 0,$$

$$i\overline{w}_e \mathrm{e}^{-\hat{\eta}} + \frac{\mathrm{d}\overline{w}_e}{\mathrm{d}\hat{\eta}} + \frac{\mathrm{d}^2\overline{w}_e}{\mathrm{d}\hat{\eta}^2} = 0, \tag{22}$$

$$(i\overline{\tau}_e - \overline{v}_e)\mathrm{e}^{-\hat{\eta}} + \frac{\mathrm{d}\overline{\tau}_e}{\mathrm{d}\hat{\eta}} + \frac{1}{\mathrm{Pr}}\frac{\mathrm{d}^2\overline{\tau}_e}{\mathrm{d}\hat{\eta}^2} = 0,$$

with the boundary conditions

$$\overline{u}_e \to 0,\ \overline{w}_e \to 1, \overline{\tau}_e \to 0 \text{ as } \hat{\eta} \to \infty.$$

No viscous heating source terms $\sim M^2$ are present in the energy equation because the mean shear of the Blasius boundary layer is negligible as the edge layer is located far from the surface.

Similarly to the incompressible case (LWG), the $z$-momentum equation (22) is decoupled from the other edge-layer equations, and can be solved independently. Its solution can be expressed in terms of Hankel function of the first kind[39]:

$$\overline{w}_e = -i^{-1/2}\pi \mathrm{e}^{-\hat{\eta}/2} H_1^{(1)}\left(2i^{1/2}\mathrm{e}^{-\hat{\eta}/2}\right). \tag{23}$$

Figure 9 shows the $|\overline{w}|$ profiles at $\overline{x} = 80$ for different $T_{dw}$ and $M = 0$ (top) and $M = 2$ (bottom). The disturbances are shown in the outer portion of the boundary layer because the edge layer is centered there at $\eta \approx 3.5$. The agreement between the edge-layer solution (23) and the boundary-region solution is very good. Similarly to the behavior at $\overline{x} = 2$ in figure 6 (bottom), an increment of $M$ and wall heating are destabilizing, while wall cooling is stabilizing. The $\mathcal{O}(1)$-coefficients on the right-hand side of equations (18) and (20) are determined by minimizing the numerical difference between the edge-layer solution and the boundary-region solution for $M = 0$ and adiabatic-wall conditions. These coefficients are 2.814 in (18) and 0.526 in (20). The same coefficients are used as the Mach number and the wall heat flux are varied. As expected, the agreement between the theoretical predictions and the numerical calculations worsens as $\eta$ decreases because the edge-layer solution is only valid for $\eta \gg 1$. A composite solution between (23) and $\overline{W}$ in (13), i.e. the solution of the WKBJ spanwise momentum equation valid for $\eta = \mathcal{O}(1)$, should be used to obtain an approximation of the numerical result which is valid throughout the whole boundary layer.

The effect of compressibility on the dominating streamwise velocity fluctuations is more intense when $\overline{x} = \mathcal{O}(1)$ than when $\overline{x} \gg 1$. This is observed in the downstream evolution of $|\overline{u}|_{max}$ as a function of $\overline{x}$ in figure 5, where the differences due to the wall heat transfer decrease as $\overline{x}$ increases. When $\overline{x} = \mathcal{O}(1)$, both the wall heat flux and the viscous heating caused by the Mach number variation affect the mean flow in the bulk of the boundary layer, and, in turn, the Klebanoff modes, which are mainly located at $\eta = \mathcal{O}(1)$. At large $\overline{x}$, the fluctuations are confined in the edge layer, and are not affected by the variations of the mean flow in the core of the boundary layer. The edge-layer disturbances are only influenced by changes of $A_F$ and $\beta_c$, which pertain to the behavior of the Blasius flow at $\eta \gg 1$ and do not vary significantly with $M$ and $T_{dw}$.

### C. Klebanoff modes for $\kappa_z = \mathcal{O}(1)$

The effect of wall heat transfer on the boundary-layer disturbances with $\kappa_z = \mathcal{O}(1)$ is investigated in this section. For these values of the spanwise wavenumber, the spanwise diffusion is of the same order of the wall-normal diffusion when $\overline{x} = \mathcal{O}(1)$, that is $\delta^* = \mathcal{O}(\lambda_z^*)$. As shown by LWG in the incompressible regime and by RW in the compressible regime, the laminar streaks reach their peak at $\overline{x} = \mathcal{O}(1)$ after an algebraic growth $\sim \overline{x}^{1/2}$. They eventually decay rapidly because of the dissipative viscous effects, which are proportional to $\kappa_z^2$ (see figure 4 at page 185 in LWG).

When $\kappa_z = \mathcal{O}(1)$, the $|\overline{u}|$ and $|\overline{\rho u}|$ fluctuations are stabilized by heating and destabilized by cooling at $\overline{x} = \mathcal{O}(1)$, as shown in the graph on the left of figure 10. The effect is more intense on $\overline{u}$ than on $\overline{\rho u}$. This scenario is opposite to the one observed for disturbances with asymptotically large spanwise wavelength, i.e. for $\kappa_z = 0$, which is studied in §III B. However, heating is destabilizing and cooling is stabilizing for small $\overline{x}$ values, so that the $\overline{u}$ trends cross one another at $\overline{x} \approx 0.0125$ and the $\overline{\rho u}$ trends do so at $\overline{x} \approx 0.5$. This is clearly pictured in the top-right and the bottom-right graphs

of figure 10, where the difference between the heat-transfer trends and the adiabatic-wall trends is shown. The reason for this lies in the fact that, even though $\kappa_z = \mathcal{O}(1)$, near the leading edge the flow is governed by the boundary-layer equations, which are recovered from the boundary-region equations when the $z$-diffusion terms are negligible. At $\overline{x} \ll 1$, the boundary layer is so thin that the wall-normal diffusion terms dominate over the spanwise diffusion terms, i.e. $\delta^* \ll \lambda_z^*$. It therefore appears clear that the concept of boundary-region behavior, for which the wall-normal diffusion balances the spanwise diffusion, is more precisely characterized by the notation $\delta^* = \mathcal{O}(\lambda_z^*)$, rather than $\kappa_z = \mathcal{O}(1)$. The later may be adopted as a rigorous definition of the boundary-region regime only at downstream locations where $\overline{x} = \mathcal{O}(1)$. The trends of the temperature fluctuations $\overline{\tau}$ do not cross in figure 10. They are similar to the $\kappa_z = 0$ case: they are destabilized by wall heating and stabilized by wall cooling at every $\overline{x}$.

Figure 11 shows that the profiles of the $\overline{u}$ and $\overline{\tau}$ fluctuations are qualitatively similar to the ones for $\kappa_z = 0$ (see figure 6). The velocity fluctuations are more influenced by the wall heat transfer when $\kappa_z = \mathcal{O}(1)$ than when $\kappa_z = 0$. The profiles of the spanwise velocity fluctuations $|\overline{w}|$ in figure 11 differs substantially from the profile for $\kappa_z = 0$ in figure 6. This is because the spanwise viscous diffusion has a significant effect in the $z$-momentum equation, and because the spanwise velocity fluctuations are driven directly by the corresponding free-stream component, which decays exponentially as $\sim \exp\left[-\left(\kappa_y^2 + \kappa_z^2\right)\overline{x}\right]$, when $\kappa_y, \kappa_z = \mathcal{O}(1)$.

The effect of the wall heat transfer on the Klebanoff modes when $\kappa_z = \mathcal{O}(1)$ or larger is confirmed by an asymptotic analysis for $\kappa_z \to \infty$, $\kappa_z/\kappa_y = \mathcal{O}(1)$. In this limit, LWG have shown that the incompressible boundary-region solutions have an asymptotic solution where the streamwise velocity component scales as $\tilde{u} = \kappa_z^2 \overline{u} = \mathcal{O}(1)$ and the streamwise coordinate is $\tilde{x} = \kappa_z^2 \overline{x} = \mathcal{O}(1)$. The compressible boundary-region equations also possess such a solution. Figure 12 shows $|\tilde{u}|_{max}$ as a function of $\tilde{x}$ at $M = 0$ for $\kappa_z = 2, 3, 4$ for wall heat transfer conditions and the adiabatic-wall condition. The trends overlap for the different values of $\kappa_z$ and the influence of wall heat transfer is confirmed. Although the analysis is valid strictly for $\kappa_z \gg 1$, the fact that the curves collapse even for $\kappa_z = 2$ validates the numerical results for $\kappa_z = \mathcal{O}(1)$.

### D. Tollmien-Schlichting waves for $\kappa_z \ll 1$

This section presents the influence of the wall-heat flux on the low-frequency TS waves discovered by RW to appear in high-Mach number subsonic and supersonic laminar boundary layers when exposed to convected gusts with $\kappa_z \ll 1$. This receptivity mechanism operates as follows.

The unsteady free-stream perturbations excite quasi three-dimensional Lam-Rott boundary-layer eigensolutions[40,41] inside the boundary layer. These disturbances evolve together with the Klebanoff modes, but, while the latter are generated and driven by the free-stream convected gusts (and thus are solutions of an inhomogeneous differential system), the former are unsteady homogeneous solutions of the boundary layer equations. Their amplitude decreases exponentially and their wavelength shortens as they evolve downstream. Goldstein[42] first discovered that these perturbations, while previously thought to be innocuous in the transition process because of their vanishingly small amplitude, play instead a crucial role in leading the boundary layer to instability. For relatively high-frequency acoustic oscillations in the free-stream, their wavelength shortening indeed causes the generation of a streamwise pressure gradient. Once this pressure gradient becomes comparable with the inertial in a very thin near-wall layer, the Lam-Rott mode evolves into an unstable, exponentially-growing TS wave. RW have shown that, when the free-stream perturbations are of low-frequency, such as the convected vortical gusts, a spanwise pressure gradient is instead generated, while the streamwise pressure gradient is negligible. The spanwise pressure gradient interferes with the viscous flow by engendering a spanwise velocity component. Once this component become of the same order of magnitude of the streamwise and wall-normal velocity components, a spatially-growing oblique TS wave is triggered. The starting location of growth can be quite close to the leading edge for Mach numbers higher than 0.8. More details on the physical mechanism are given

in RW, and a small schematic of the TS-wave generation is shown in the bottom-right corner of figure 1.

Figure 13 shows the downstream evolution of $|\overline{u}|_{max}$ for $M = 0.8$ (top) and 3 (bottom), different wall heat transfer conditions and $\kappa_z = 0.02$. At $\overline{x} = \mathcal{O}(1)$, the Klebanoff modes dominate the boundary layer and the wall heat flux has a similar effect to the one for $\kappa_z = 0$, i.e. cooling is stabilizing and heating is destabilizing, for both subsonic and supersonic conditions (see §III B). The disturbances eventually evolve into exponentially-growing, oblique TS waves. Cooling shifts downstream the location at which the waves start growing, while heating has the opposite effect. The wall heat flux is more influential in subsonic conditions and it affects the growth rate only slightly. As the TS waves we consider are of low-frequency because they are induced by the Klebanoff modes through the triggering of the Lam-Rott modes, they are identified as compressible first modes[5], for which wall cooling has been confirmed to be stabilizing, both numerically[34,43–46] and experimentally[47,48].

In figure 14, the real part of $\overline{u}$ as a function of the downstream distance represents the wave packet of the growing disturbance. The conditions are the same as in figure 13, i.e. $M = 3$, different wall heat fluxes and $\kappa_z = 0.02$. The waves undergo an intense amplification, reach a peak, and eventually decay at almost the same rate of the growth. Once established, the waves possess a well-defined streamwise wavelength, which are only slightly affected by the compressibility effects. The maximum peak is only slightly shifted downstream as $T_{dw}$ decreases. Wall cooling has a dramatic effect on the maximum amplitude of the wave, while heating is less influential. The amplitude peak decreases by two orders of magnitude from $|\overline{u}|_{max} \approx 470$ to $|\overline{u}|_{max} \approx 7$ for cooling ($T_{dw} = 0.2$) when compared to adiabatic-wall conditions, while the same amount of wall heating ($T_{dw} = -0.2$) only augments the peak by one order of magnitude to $|\overline{u}|_{max} \approx 4700$.

The growing disturbance is investigated in more detail by studying its growth rate and wavenumber. These can be extracted from the numerical calculations as the real and the imaginary parts of the ratio $\overline{u}_x/\overline{u}$, where in this section the subscript $x$ indicates the partial derivative with respect to $\overline{x}$. These quantities may be also determined by triple-deck asymptotic analysis. The interested reader should refer to RW for further details. The location of growth $\overline{x}_c$ is found to occur for $\kappa_z \ll 1, \overline{x} \gg 1$ where

$$\kappa_z \overline{x}_c = \mathcal{O}(1),$$

so that the new streamwise coordinate $x_1 = \kappa_z \overline{x} = \mathcal{O}(1)$ is introduced. The streamwise velocity component is assumed to grow as follows

$$\overline{u} \sim \exp\left[\frac{i}{\kappa_z^{1/2}} \int_0^{\overline{x}} \alpha_1(x_1) \mathrm{d}\breve{x}\right].$$

The growth rate and the wavenumber are thus found as $-\Im(\alpha_1)/\kappa_z^{1/2}$ and $\Re(\alpha_1)/\kappa_z^{1/2}$, respectively. The complex wavenumber $\alpha_1 = \alpha_1(x_1)$ is determined through the dispersion relation[49,50]

$$\Delta(x_1, \alpha_1) \equiv \int_{\eta_0}^{\infty} \mathrm{Ai}(\breve{\eta}) \mathrm{d}\breve{\eta} - \frac{\mu(0)^{1/3}}{T(0)^{7/3}} \left(\frac{F''(0)}{\sqrt{2x_1}}\right)^{5/3} (i\alpha_1)^{-1/3} \mathrm{Ai}'(\eta_0) = 0, \tag{24}$$

where Ai indicates the Airy function of the first kind, the prime denotes its first derivative, and

$$\eta_0 = -(\alpha_1 F''(0))^{-1} \left(2iF''(0)\alpha_1 x_1 T(0)/\mu(0)\right)^{1/3}.$$

Compressibility is at work in (24) through the wall quantities $\mu(0)$, $T(0)$ and $F''(0)$. Differently from the receptivity studies by Smith[49] and Wu[50], the relation (24) does not contain the $\alpha_1^2$ term because the streamwise pressure gradient is not active in the instability process described by the boundary-region equations. Another important feature revealed by the triple-deck analysis is that the integral term denotes the effect of the spanwise pressure gradient induced by the wavelength

shortening of the Lam-Rott mode. In RW, it is shown that this term vanishes as $x_1 \to 0$, thereby allowing the TS wave to match the Lam-Rott mode upstream.

The numerical calculations are validated by the triple-deck analysis for $\kappa_z = 0.0005$. This value is small enough to allow for a quantitative validation of the numerical data by the triple-deck data because the approximation given by the latter improves as $\kappa_z$ decreases. In figure 15, a comparison between the boundary-region solutions and the triple-deck results computed by equation (24) is shown for the wavenumber and the growth rate of the disturbances for $M = 3$ and different wall heat transfer conditions. A quite violent transient phase is observed through which the disturbances adjust from the long-wavelength, decaying behavior of the Klebanoff modes to the short-wavelength, exponentially-growing regime of the TS wave. Both the growth rate and wavenumber vary slowly with $\overline{x}$ once the instability has developed. As marked by the black dots in the bottom graph of figure 15, wall cooling moves the starting location of instability further downstream and slightly decreases the growth rate there, while heating has the opposite destabilizing effect. As displayed by the top graph of figure 15, the wavelength only marginally decreases by removing heat and, similarly to what observed for the maximum amplitude, the effect of cooling in affecting the TS waves is slightly more significant than wall heating. The triple-deck data are consistent with the boundary-region data and the wavenumbers are predicted quantitatively more accurately than the growth rates.

## IV. SUMMARY

The response of low-frequency disturbances in a compressible laminar boundary layer to wall heat transfer has been investigated numerically and by perturbation methods. The thermal Klebanoff modes, namely the streamwise-elongated fluctuations of vorticity and temperature appearing in the core of the boundary layer through the continuous action of free-stream disturbances, are stabilized by wall cooling when the spanwise diffusion effects are negligible, while the opposite occurs when the spanwise length scale is comparable with the boundary-layer thickness.

The oblique Tollmien-Schlichting waves, induced by an unsteady, wavelength-shortening receptivity mechanism and appearing only when the free-stream velocity is comparable with the speed of sound, are significantly suppressed when wall cooling is applied. The neutral point of instability is considerably moved downstream, whereas the growth rate and the streamwise length scale of the waves are less influenced by the compressibility effects.

Figure 16 schematically depicts the flow regimes and the effects of the wall heat flux on the low-frequency disturbances for different $\overline{x}$ and $\kappa_z$. The circles indicate whether wall cooling or wall heating stabilizes the disturbances, and whether the effect is mild or significant. The wall heat transfer is generally more influential when $\overline{x} = \mathcal{O}(1)$ than when $\overline{x} \gg 1$, except when $\kappa_z \gg 1$ because the fluctuations are strongly attenuated by viscous effects, and in the TS-wave regime, for which cooling significantly shifts $\overline{x}_c$ downstream when $\overline{x} \gg 1$. $\kappa_z \approx 0.03$ represents the highest value of the spanwise wavenumber at which TS waves may be observed: their growth is suppressed by the viscous action of the Klebanoff modes for higher $\kappa_z$ values. Note that, if $\kappa_z$ is slightly lower than 0.03 and nonlinear effects are not influential, then the Klebanoff modes may be observed both upstream and downstream of the TS wave. The starting location for instability $\overline{x}_c$ is inversely proportional to $\kappa_z$ only for very small values of $\kappa_z$, while it is approximately constant when $\kappa_z = 0.01 - 0.03$. As outlined in RW, the $\overline{x}_c \sim \kappa_z^{-1}$ relation is not expected to be valid for finite $\kappa_z$ values, for which the exact relation between $\overline{x}_c$ and $\kappa_z$ depends on the external forcing, namely on $\kappa_y$.

In line with Mack[43], this work outlines the importance of the precise specification of the external perturbations to understand how the streaks may be controlled by the wall heat flux. Because the response of the low-frequency disturbances to the heat transfer depends on the relative magnitude of the free-stream wavelengths with respect to the boundary-layer thickness, detailed information of the oncoming free-stream energy spectrum is necessary for the design of a wall-based, thermal controller.

**Acknowledgments**

P. Ricco would like to thank Professor Xuesong Wu for the PhD supervision of part of this work and Dr Andrea Ducci for his help with the editing of the figures. D. L. Tran acknowledges the hospitality of King's College London, where he spent his research visit from May through August 2008.

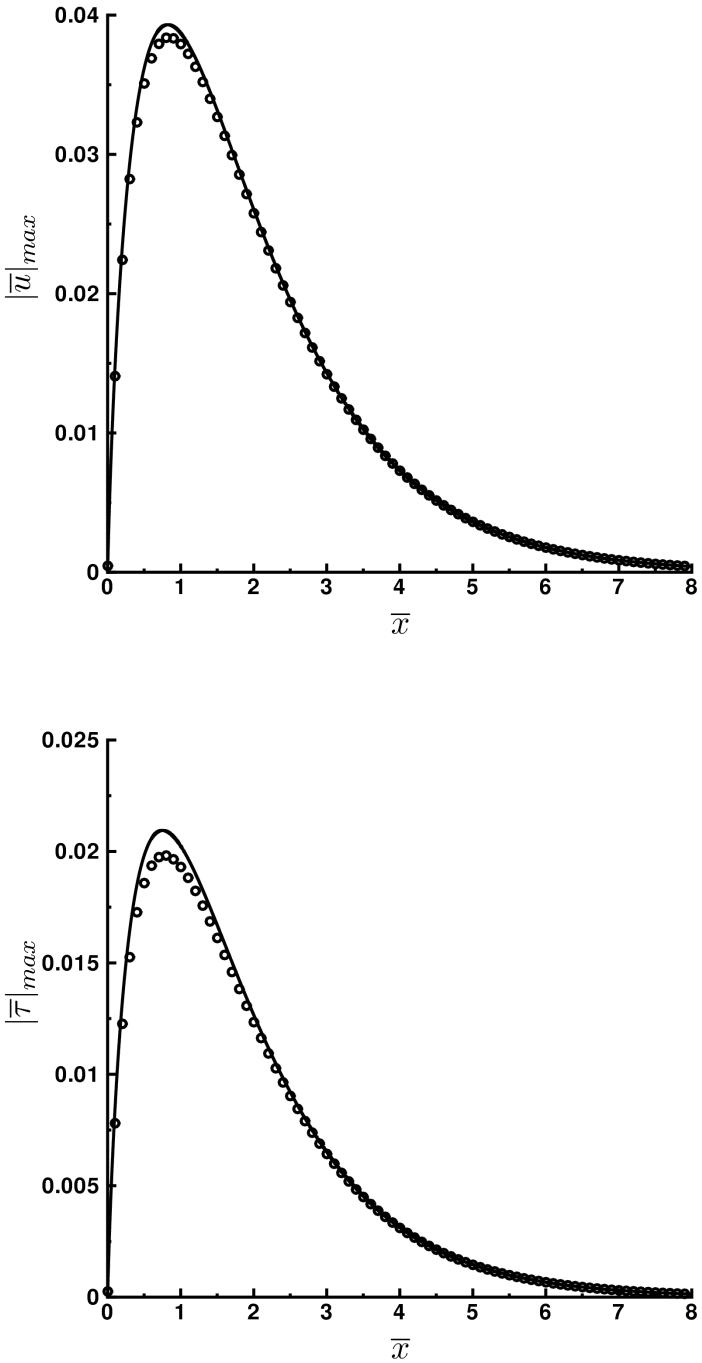


FIG. 3: Maximum (across $\eta$) of the streamwise velocity (top) and temperature fluctuation (bottom) for $M$=2, $T_{dw} = 0.2$ and $\kappa_z = 1$.

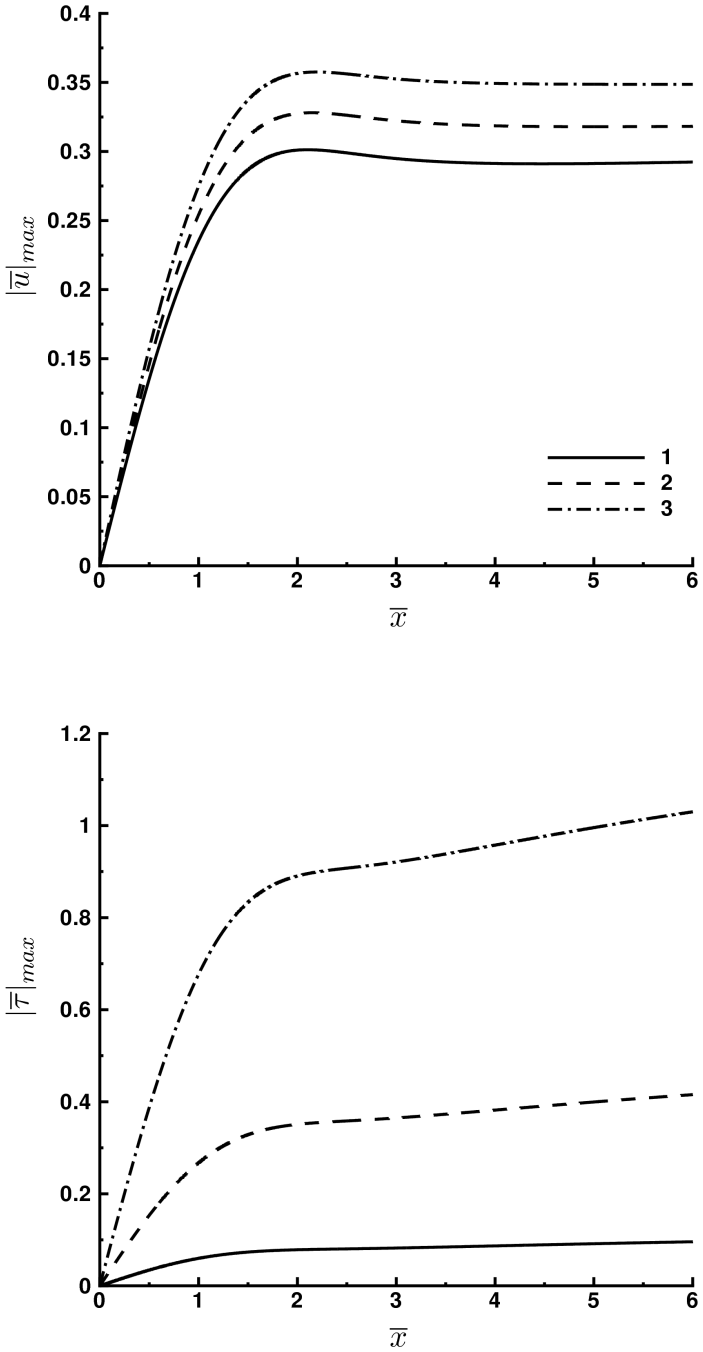


FIG. 4: Maximum (along $\eta$) of velocity (top) and temperature (bottom) fluctuations for different Mach numbers, adiabatic-wall conditions and $\kappa_z = 0$.

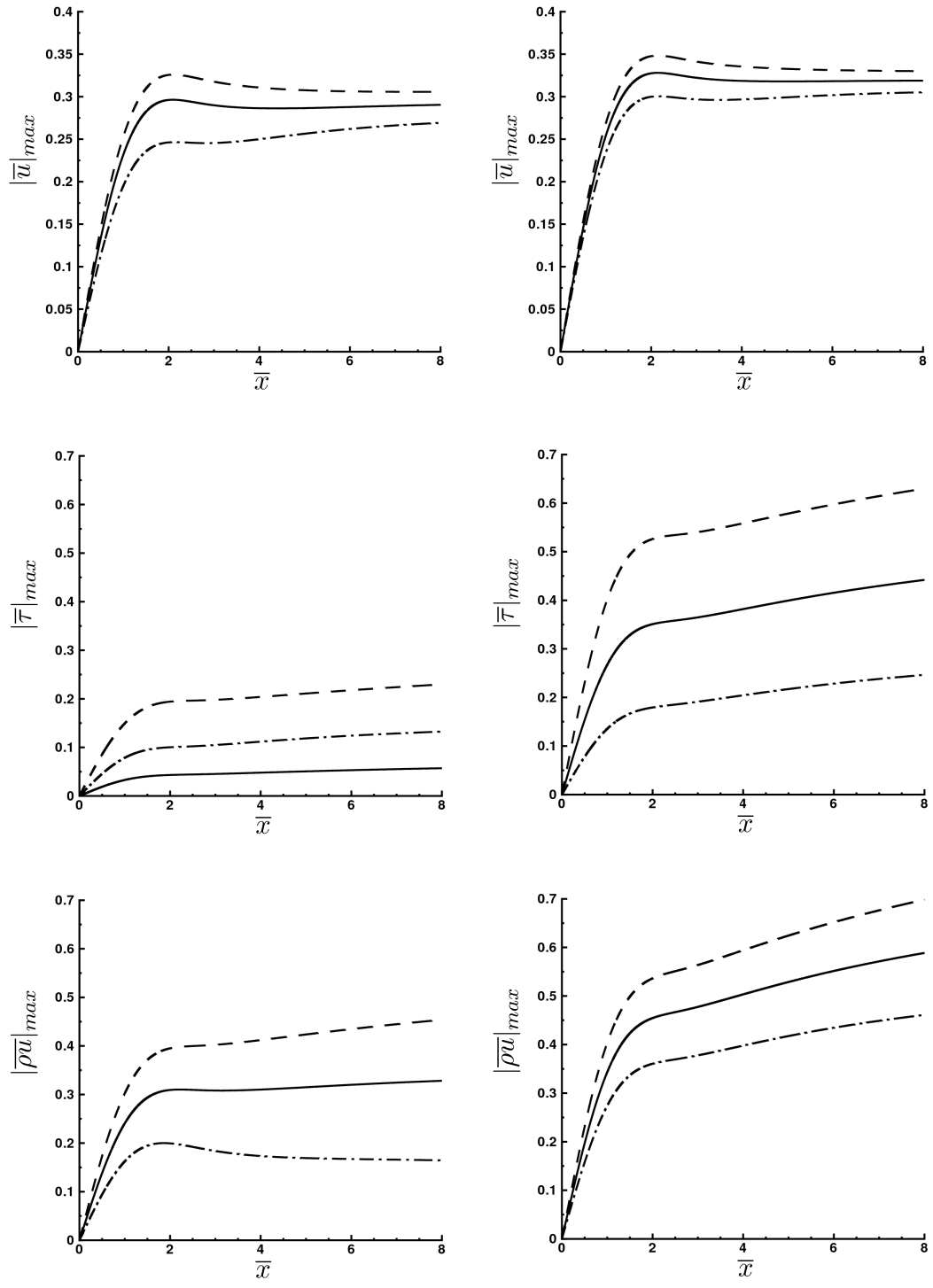


FIG. 5: Maximum (along $\eta$) of streamwise velocity (top), temperature (middle) and mass-flux fluctuations (bottom) for $M$=0.75 (left), $M$=2 (right) and $\kappa_z = 0$.

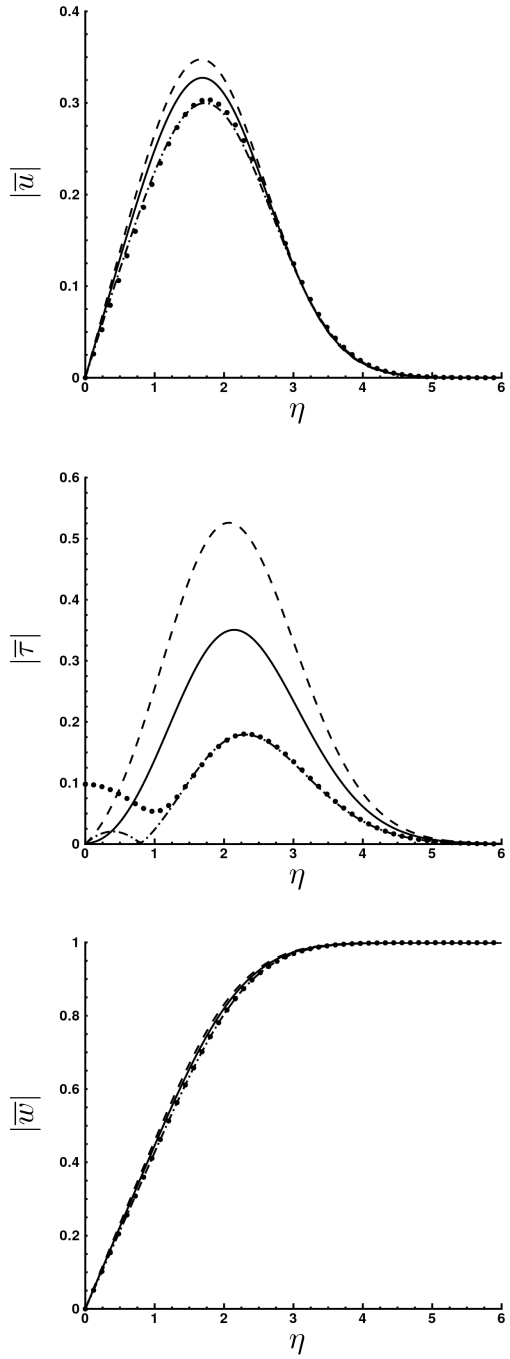


FIG. 6: Streamwise velocity (top), temperature (middle) and spanwise (bottom) velocity fluctuations for $M$=2 at $\overline{x} = 2$ for $\kappa_z = 0$. The black circles indicate the solutions obtained by the Neumann wall boundary condition on $\overline{\tau}$ (every four data point is plotted).

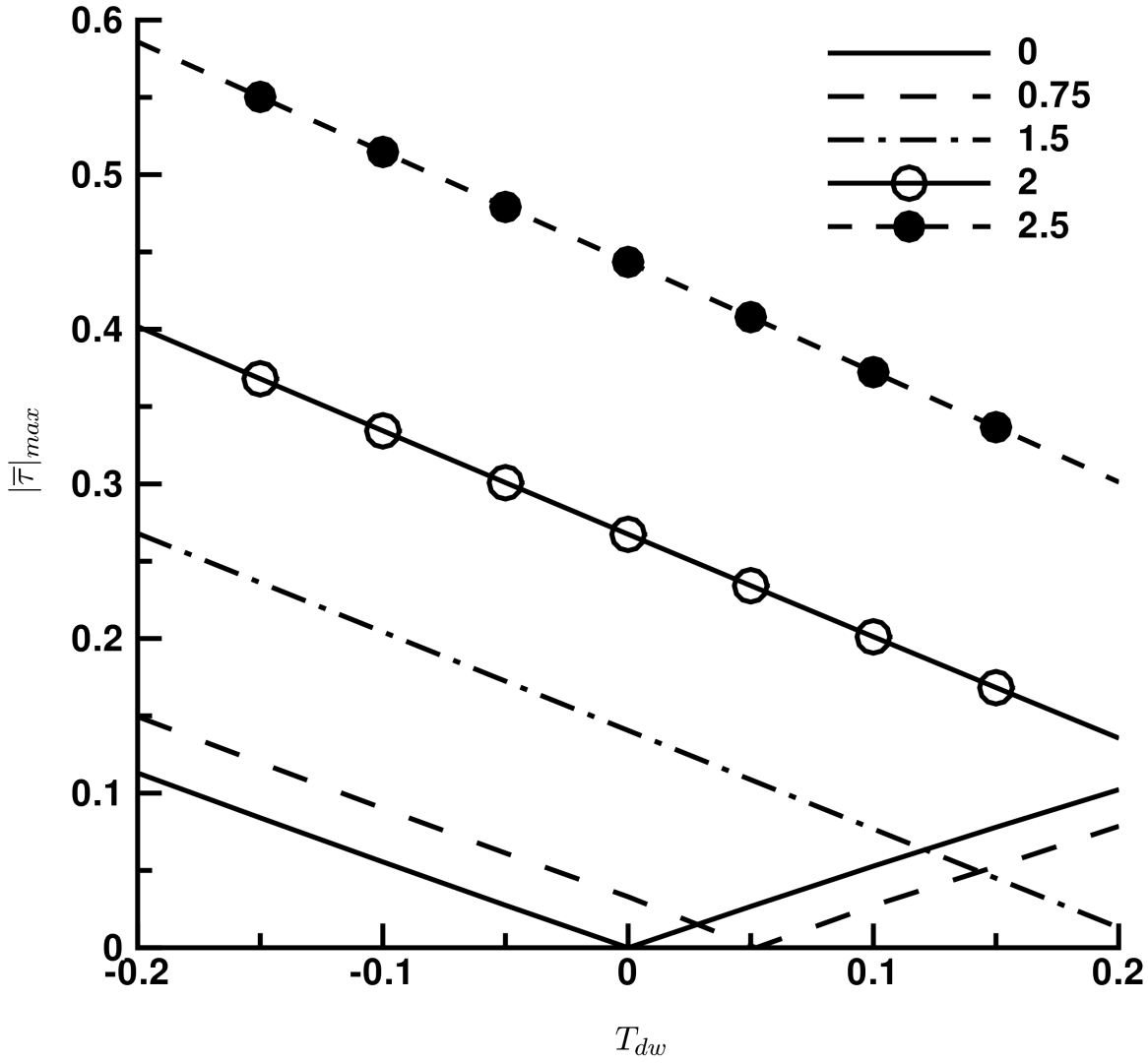


FIG. 7: Maximum (along $\eta$) of temperature fluctuations at $\overline{x}$=1 for $\kappa_z = 0$ as a function of $T_{dw}$ for different Mach numbers (see legend in graph).

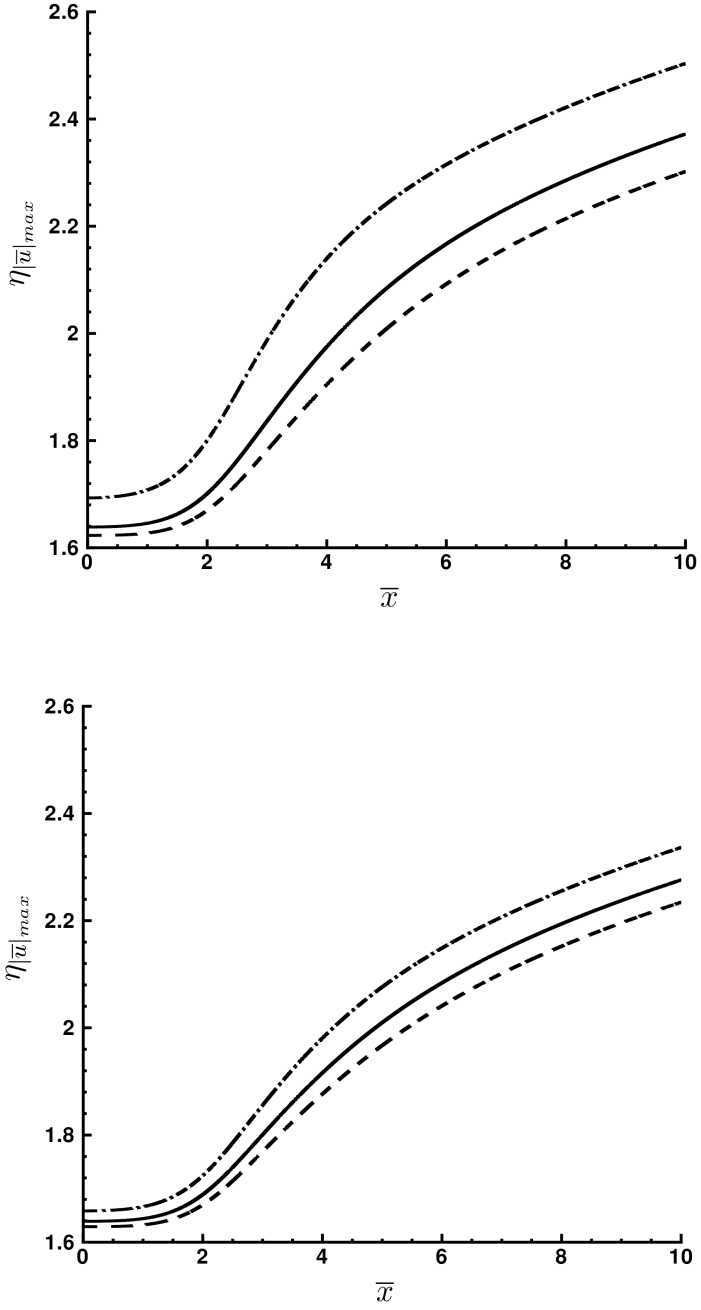


FIG. 8: Wall-normal position $\eta$ of the streamwise velocity maximum for $M$=0.75 (top), $M$=2 (bottom) and $\kappa_z = 0$.

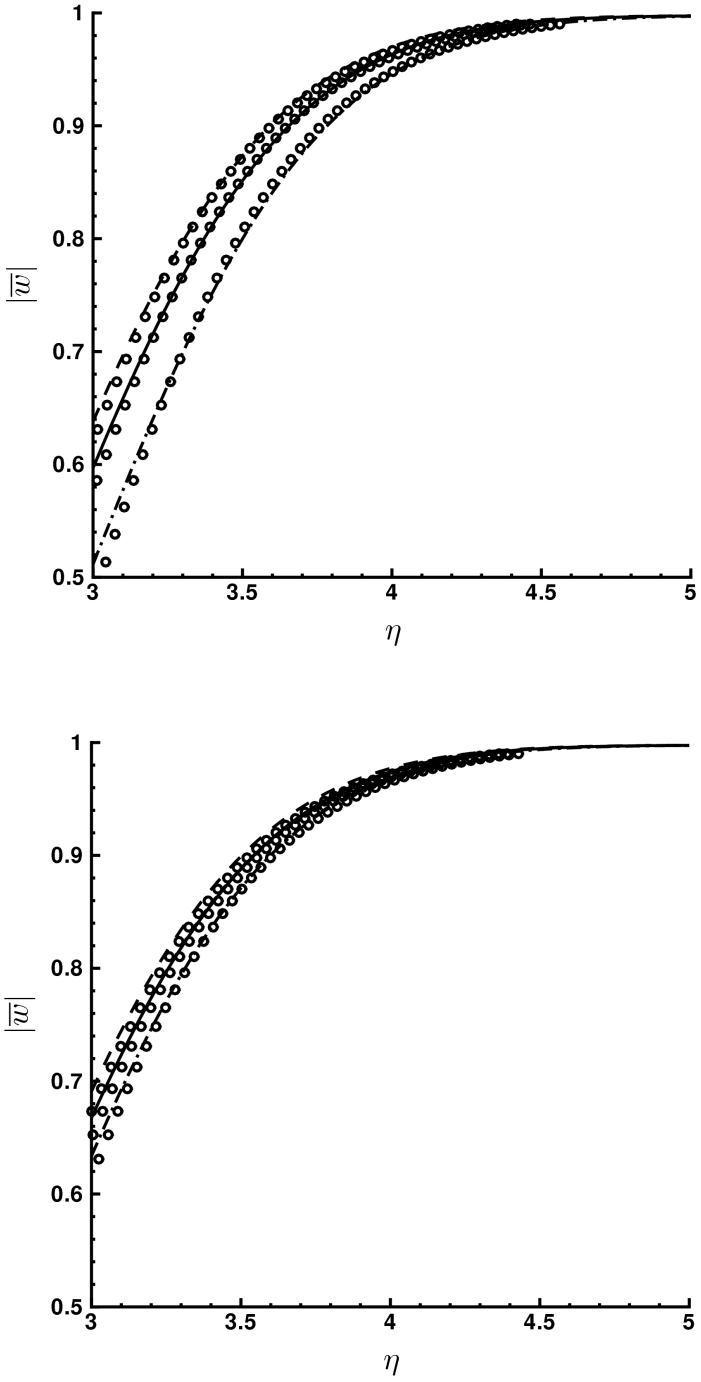


FIG. 9: Spanwise velocity fluctuations at $\overline{x} = 80$ for $\kappa_z = 0$ for $M = 0$ (top) and $M = 2$ (bottom). The circles indicate the edge-layer solutions and the lines represent the boundary-region solutions.

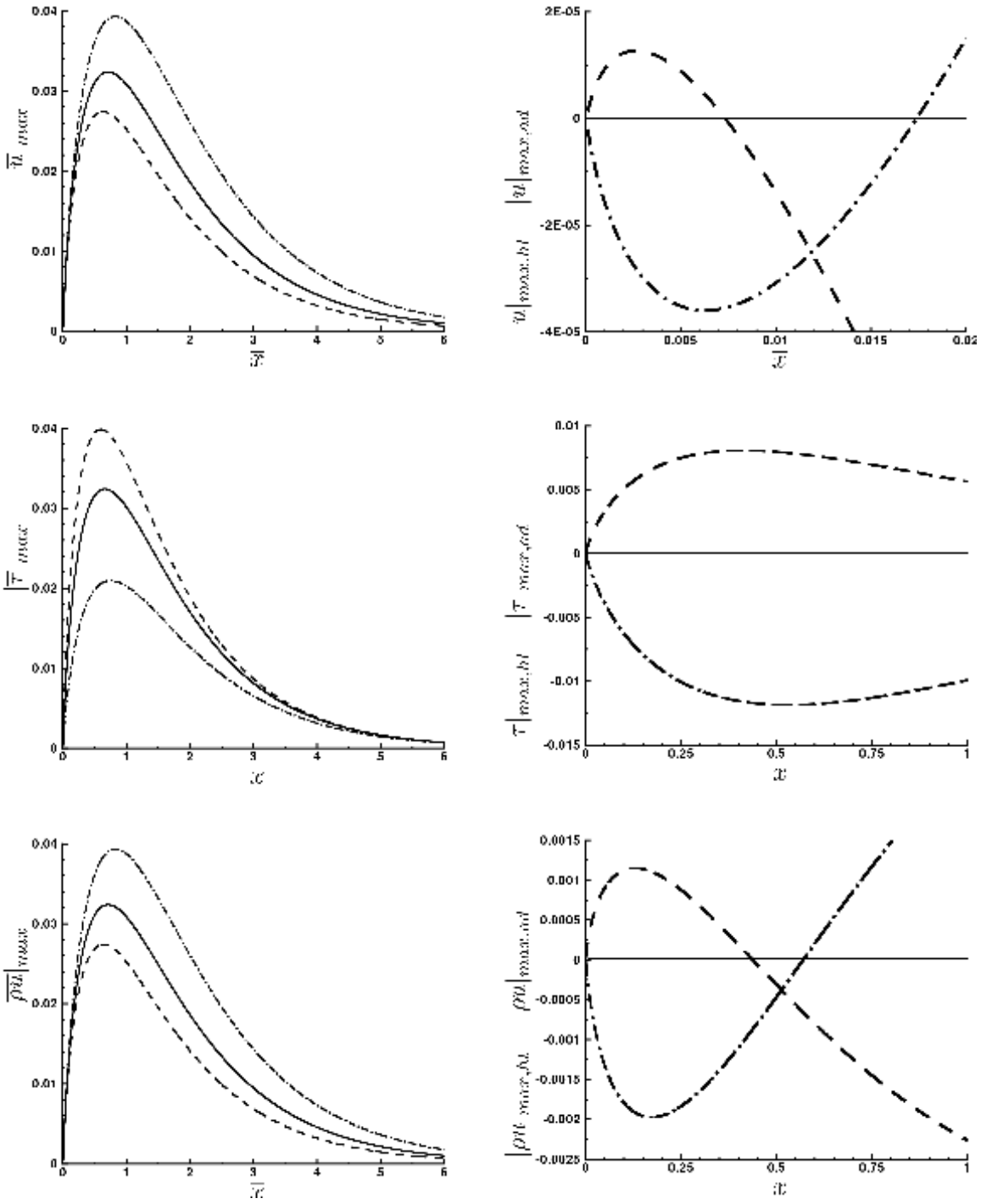


FIG. 10: Maximum (along $\eta$) of streamwise velocity (top-left), temperature (middle-left) and mass-flux fluctuations (bottom-left) as functions of $\overline{x}$ for $M = 2$ and $\kappa_z = 1$. The thick-line graphs on the right present the difference between the heat-flux curves (denoted by subscript $ht$) and the adiabatic-wall curves (indicated by subscript $ad$).

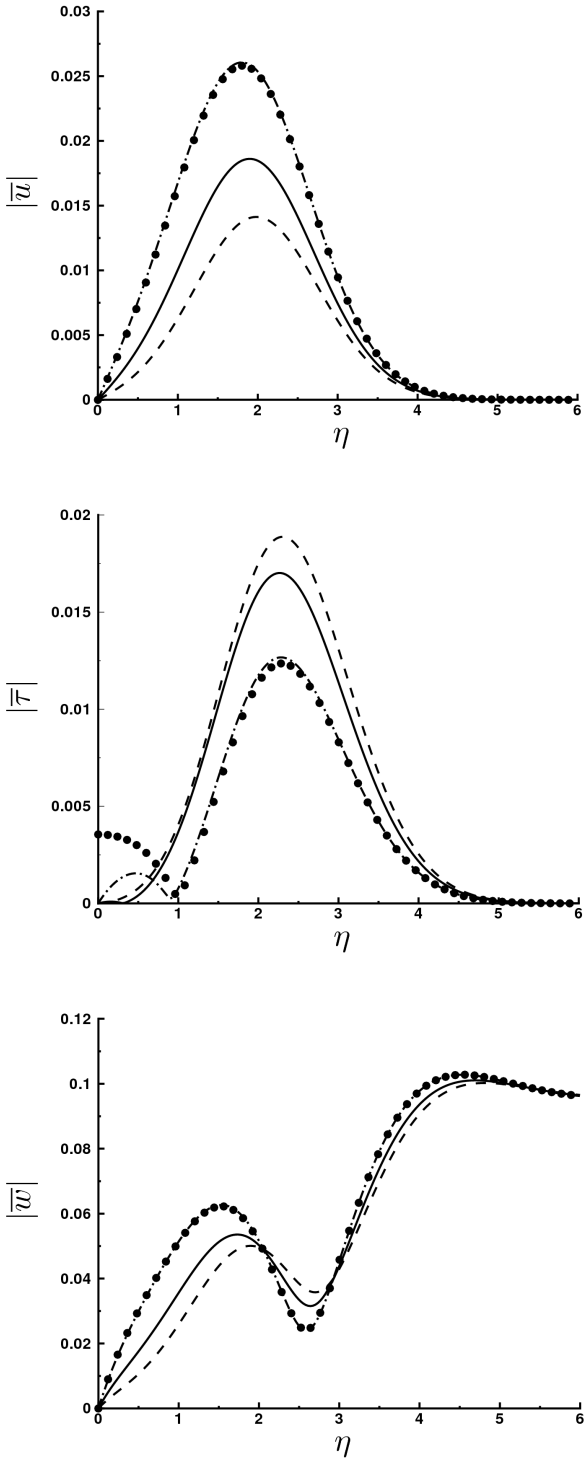


FIG. 11: Streamwise velocity (top), temperature (middle) and spanwise velocity (bottom) for $M = 2$ at $\overline{x} = 2$ for $\kappa_z = 1$. The black circles indicate the solutions obtained by the Neumann wall boundary condition on $\overline{\tau}$ (every four data point is plotted).

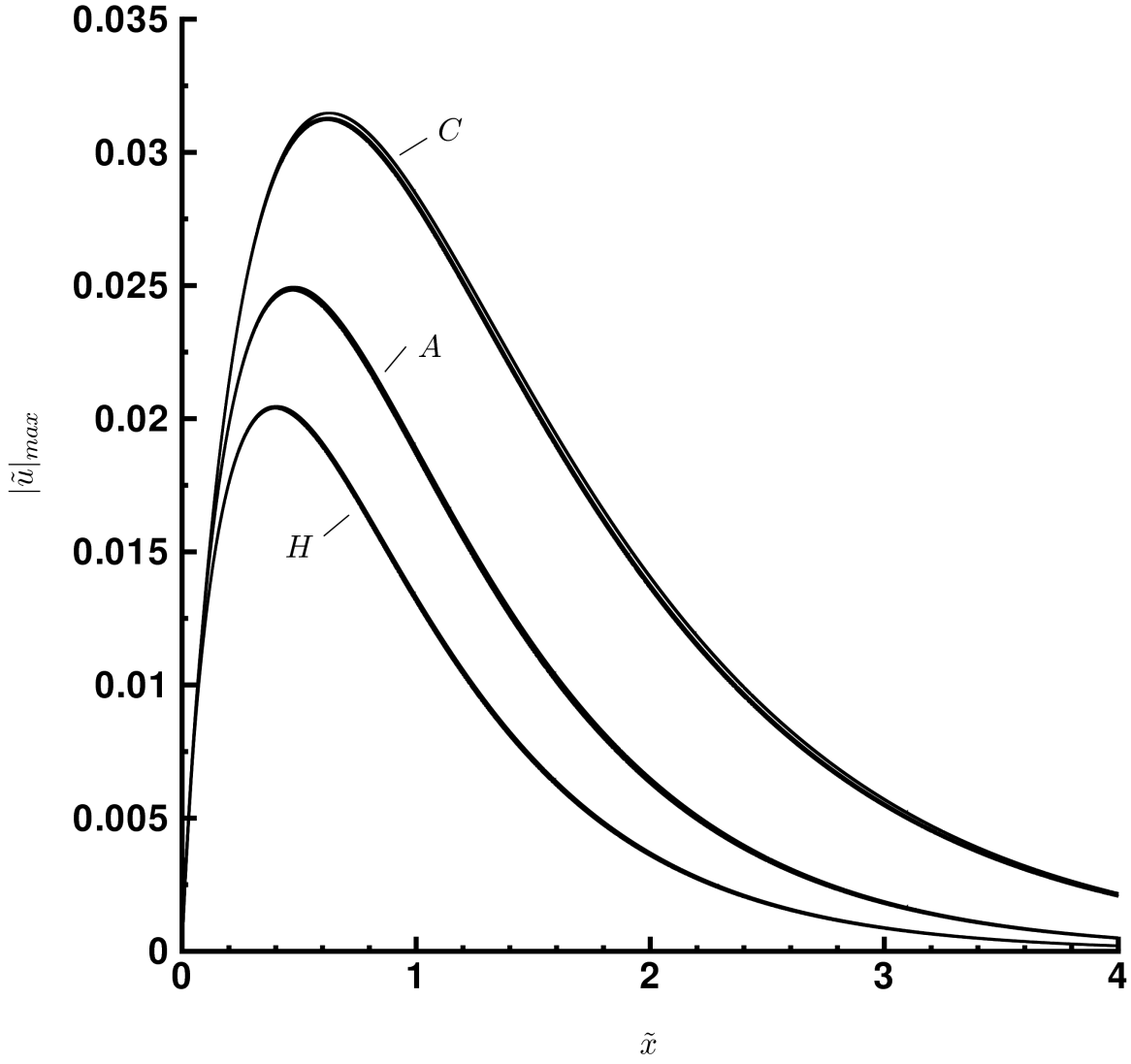


FIG. 12: Streamwise velocity $|\tilde{u}|_{max} = \kappa_z^2 |\overline{u}|_{max}$ as a function of $\tilde{x} = \kappa_z^2 \overline{x}$ for wall-heating ($T_{dw} = -0.2, H$), adiabatic-wall ($T_{dw} = 0, A$), and wall-cooling conditions ($T_{dw} = 0.2, C$) at $M = 0$. Results for $\kappa_z = 2, 3, 4$ are shown.

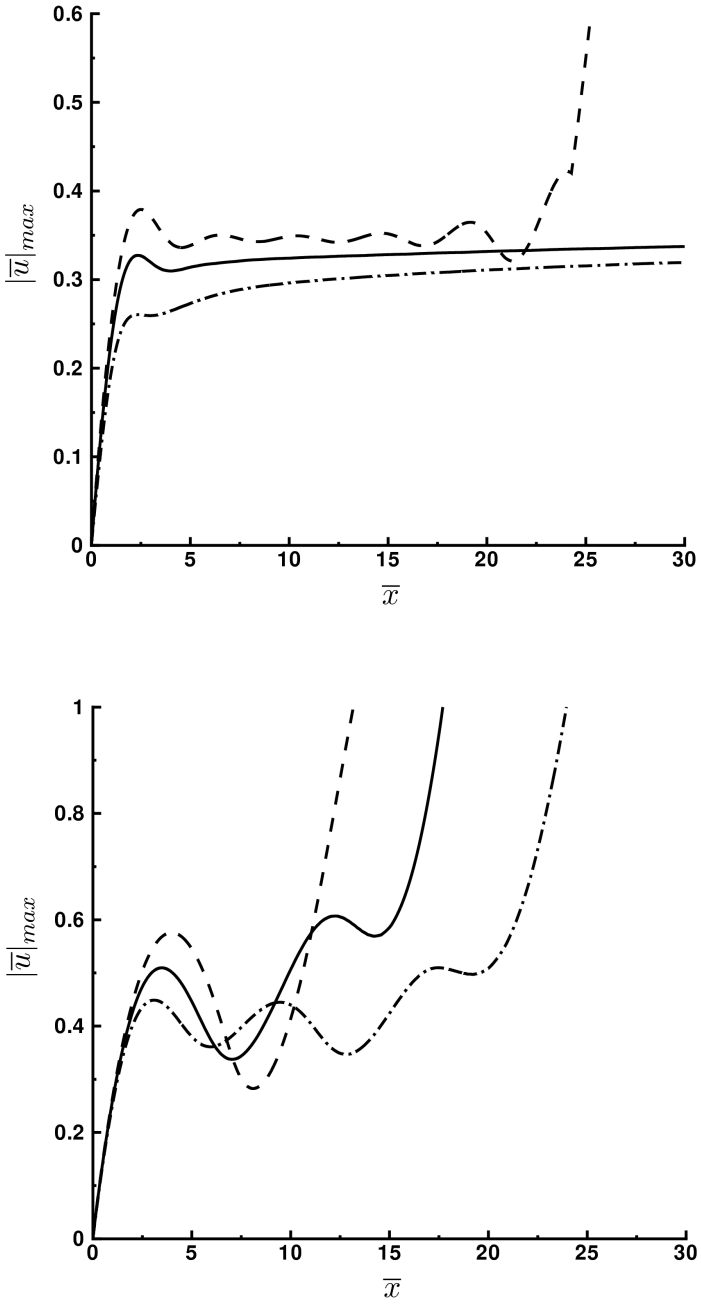


FIG. 13: Maximum of streamwise velocity component as a function of $\overline{x}$ for $\kappa_z = 0.02$ and $M = 0.8$ (top) and $M = 3$ (bottom) for $T_{dw} = -0.2, 0, 0.2$.

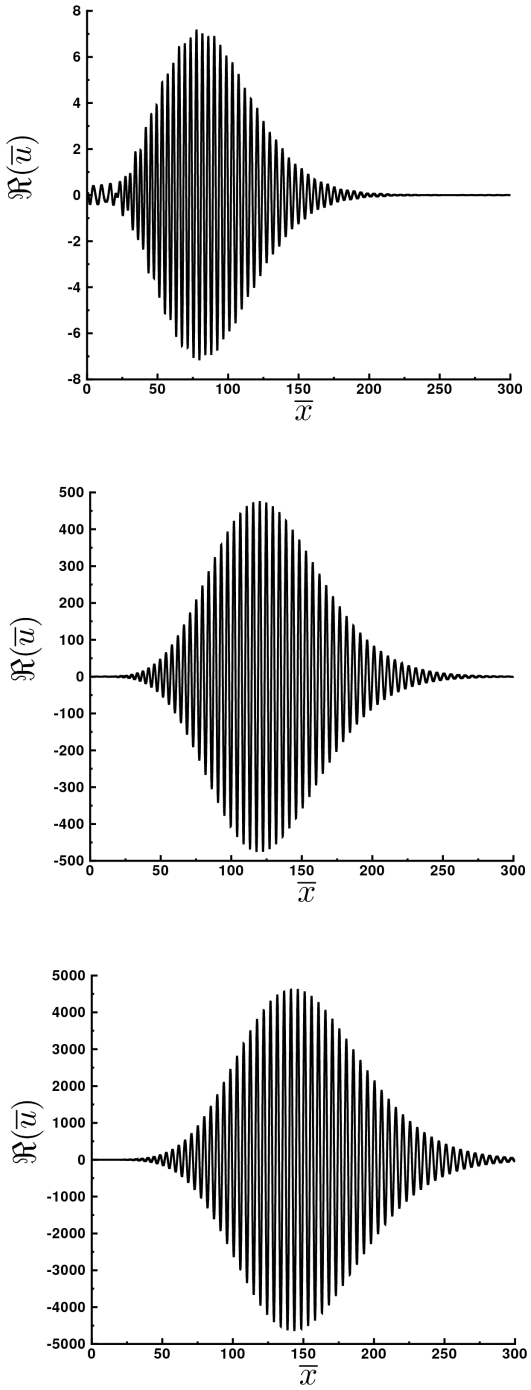


FIG. 14: Real part of streamwise velocity component $\overline{u}$ at $\eta = 2$ as a function of $\overline{x}$ for $M = 3$, $\kappa_z = 0.02$ for wall cooling ($T_{dw} = 0.2$ - top), adiabatic wall ($T_{dw} = 0$ - middle) and wall heating ($T_{dw} = -0.2$ - bottom).

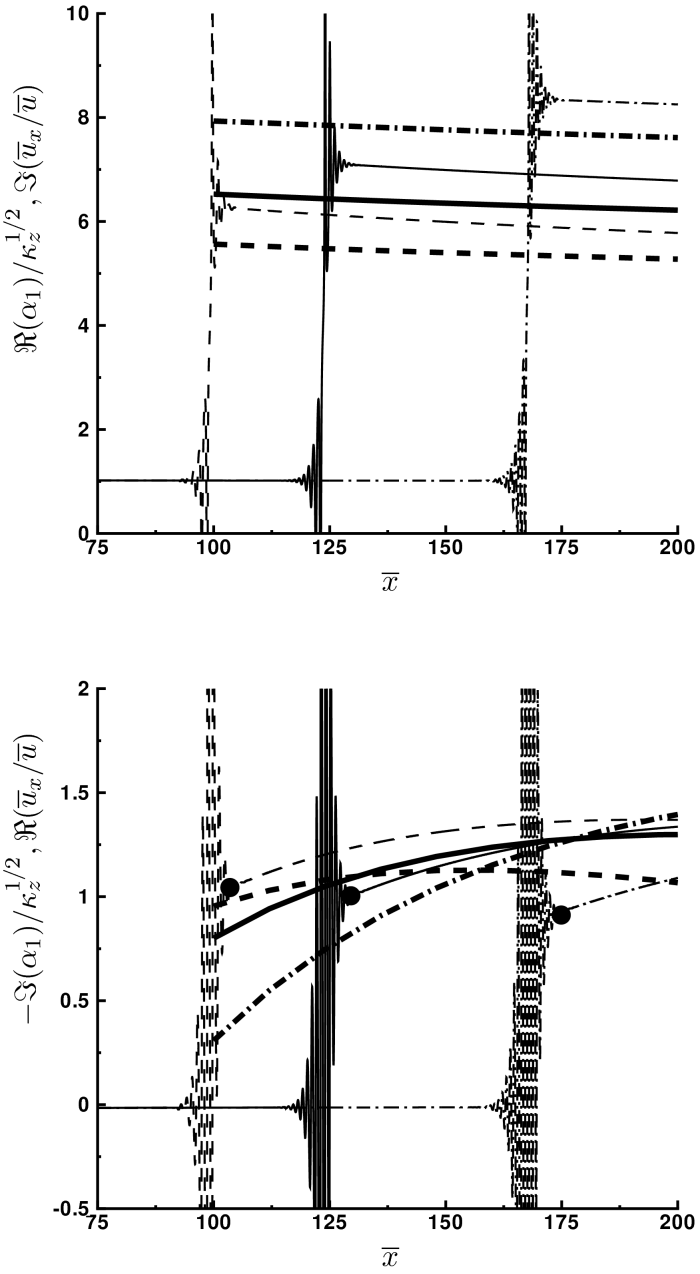


FIG. 15: Comparison of the wavenumber (top) and growth rate (bottom) of the growing disturbances for $M = 3$ and $\kappa_z = 0.0005$. The thin lines indicate the boundary-region solutions and the thick lines denote the triple-deck solutions. Wall heat-transfer conditions are for $T_{dw} = -0.2, 0, 0.2$. The black dots indicate the growth rates and starting location of the instability.

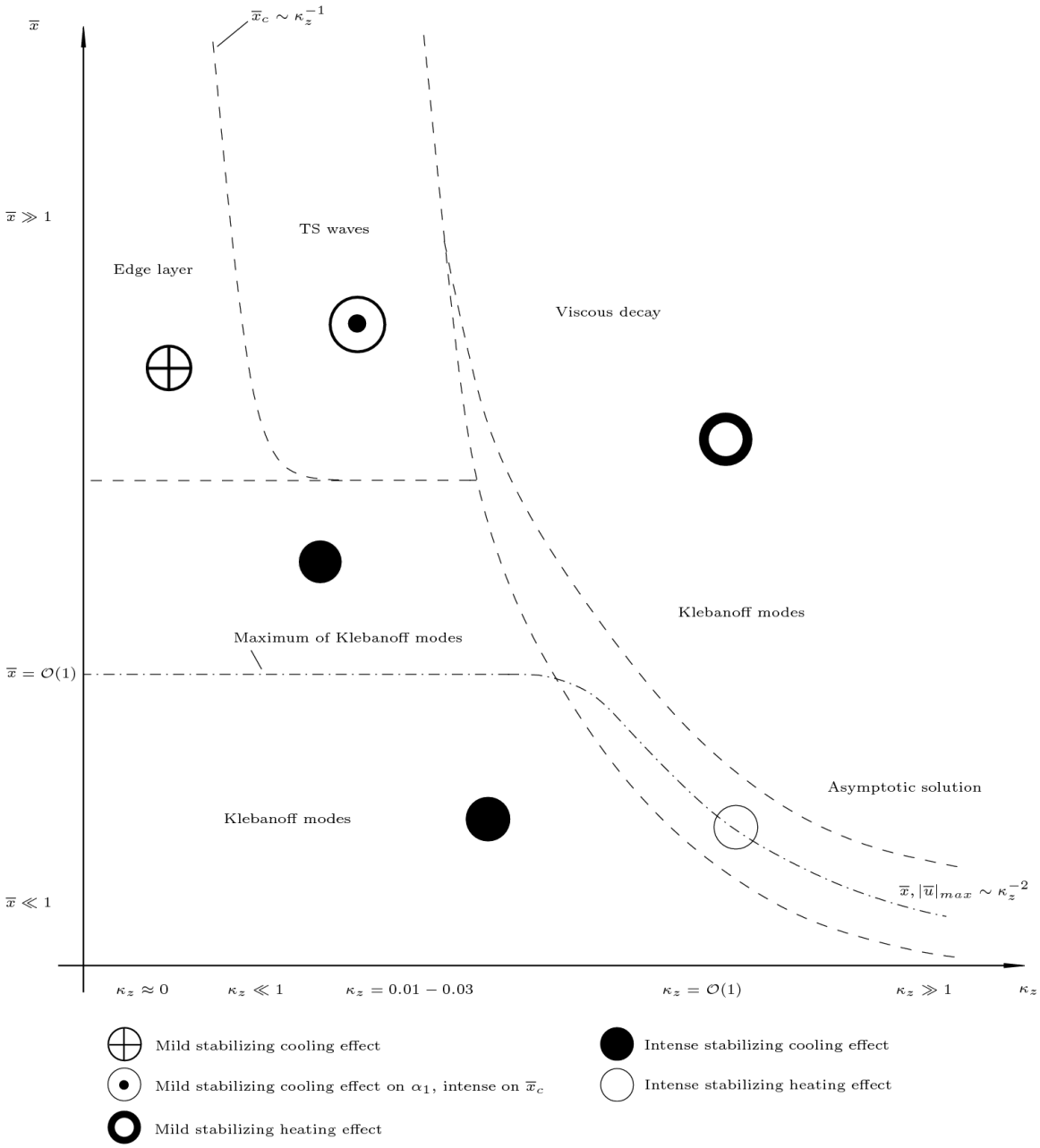


FIG. 16: Schematic of the flow regimes and the wall heat transfer effects on the streamwise velocity fluctuations for constant $\lambda_x^*$, $M = \mathcal{O}(1)$ and $\kappa_z = \kappa_y$.

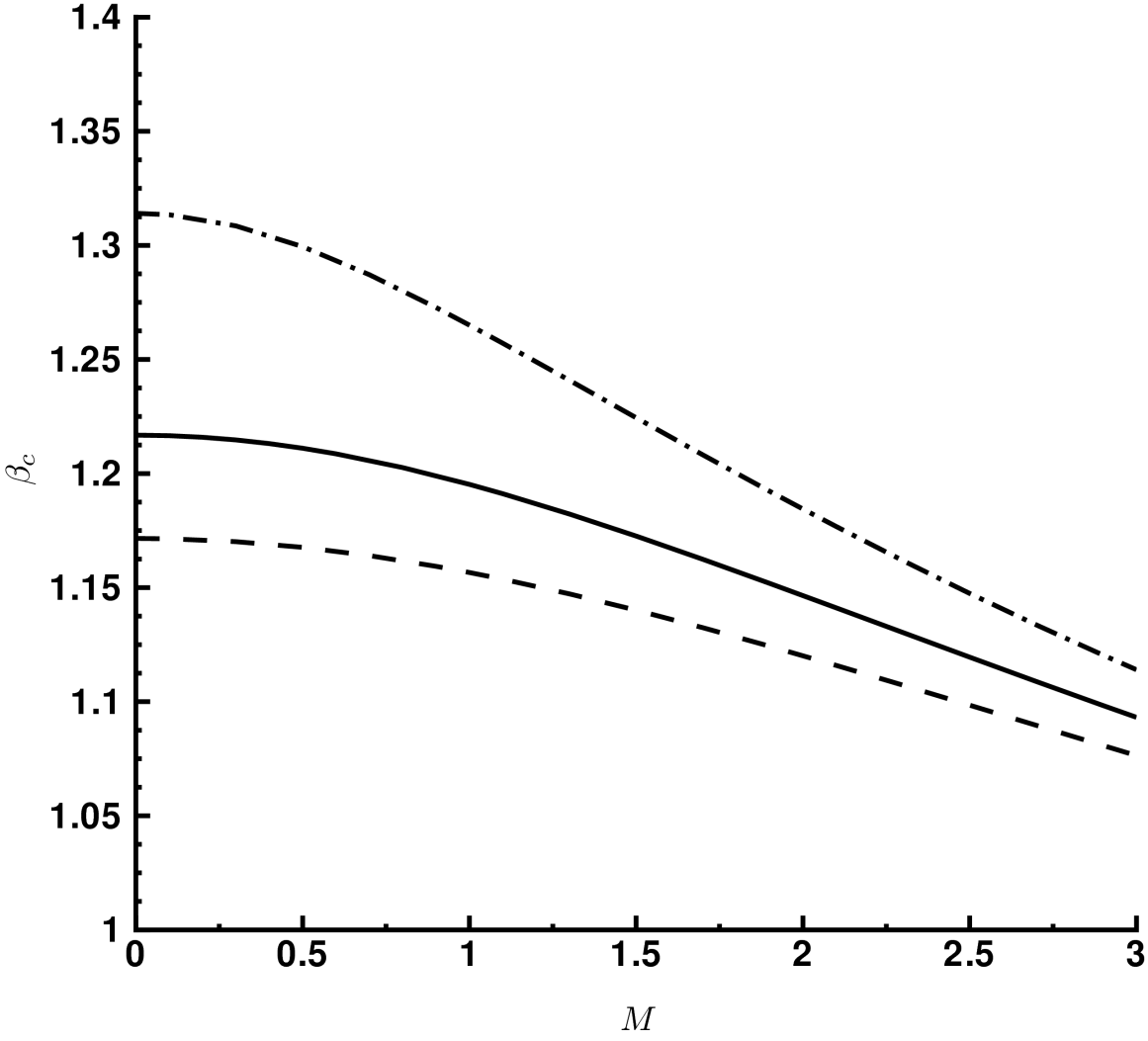


FIG. 17: $\beta_c$ as function of Mach number for $T_{dw} = -0.2, 0, 0.2$.

**Appendix: Definition and properties of $\beta_c$, $A_F$ and $A_T$.**

The quantities $\beta_c$, $A_F$ and $A_T$ are defined and their dependence on $M$ and $T_{dw}$ is studied. Note that, while $A_F$ appears in the edge-layer analysis in §III B, $A_T$ is not used throughout the paper, but it is included here for completeness. $A_F$ pertains to the behavior of the mean streamwise velocity profile in the outer portion of the boundary layer, and $A_T$ is its analogous for the mean temperature profile.

$\beta_c$ is defined as follows:

$$\beta_c = \lim_{\eta\to\infty} (\eta - F).$$

Figure 17 shows the behavior of $\beta_c$ as a function of $M$ and $T_{dw}$. Both an increment of $M$ and of the wall heating yield lower $\beta_c$ values, while cooling has the opposite effect. In order to define $A_F$ and $A_T$, the asymptotic behavior of $F$ and $T$ for $\eta \gg 1$ is studied. In this limit,

$$F = \overline{\eta} + \tilde{f}, \quad T = 1 + \tilde{T},$$

where $\tilde{f}, \tilde{T} \ll 1$. Inserting these expressions into (3) and (4), and neglecting the nonlinear terms involving $\tilde{f}$, $\tilde{T}$ and their derivatives, one finds

$$\overline{\eta}\tilde{f}'' + \tilde{f}''' = 0, \quad \mathrm{Pr}\,\overline{\eta}\,\tilde{T}' + \tilde{T}'' = 0.$$

It then follows that for $\eta \gg 1$,

$$F \to \overline{\eta} + \frac{A_F}{\overline{\eta}^2}\mathrm{e}^{-\overline{\eta}^2/2}, \tag{25}$$

$$T \to 1 - \frac{A_T}{\overline{\eta}}\mathrm{e}^{-\mathrm{Pr}\overline{\eta}^2/2}.$$

By differentiation of (25), $A_F$ can be expressed as

$$A_F = \lim_{\eta\to\infty} F''\mathrm{e}^{\overline{\eta}^2/2},$$

and integration by parts gives

$$\int_0^\infty F'''\mathrm{e}^{\overline{\eta}^2/2}\mathrm{d}\eta = \lim_{\eta\to\infty} F''\mathrm{e}^{\overline{\eta}^2/2} - F''(0)\mathrm{e}^{\beta_c^2/2} - \int_0^\infty F''(0)\,\overline{\eta}\,\mathrm{e}^{\overline{\eta}^2/2}\mathrm{d}\eta.$$

It then follows that

$$A_F = F''(0)\mathrm{e}^{\beta_c^2/2} + \int_0^\infty (F''' + \overline{\eta}\,F'')\mathrm{e}^{\overline{\eta}^2/2}\mathrm{d}\eta.$$

By a similar procedure, $A_T$ is found as

$$A_T = \lim_{\eta\to\infty} T'\mathrm{e}^{\mathrm{Pr}\overline{\eta}^2/2} = \int_0^\infty (T'' + \overline{\eta}\,T'\,\mathrm{Pr})\,\mathrm{e}^{\mathrm{Pr}\,\overline{\eta}^2/2}\mathrm{d}\eta + T'(0)\,\mathrm{e}^{\mathrm{Pr}\beta_c^2/2}.$$

The dependence of $A_F$ and $A_T$ on the Mach number and the wall heat flux is shown in figure 18. Both wall heating and an increase of $M$ lead to lower $A_F$ and $A_T$ values, while wall cooling has the opposite effect.

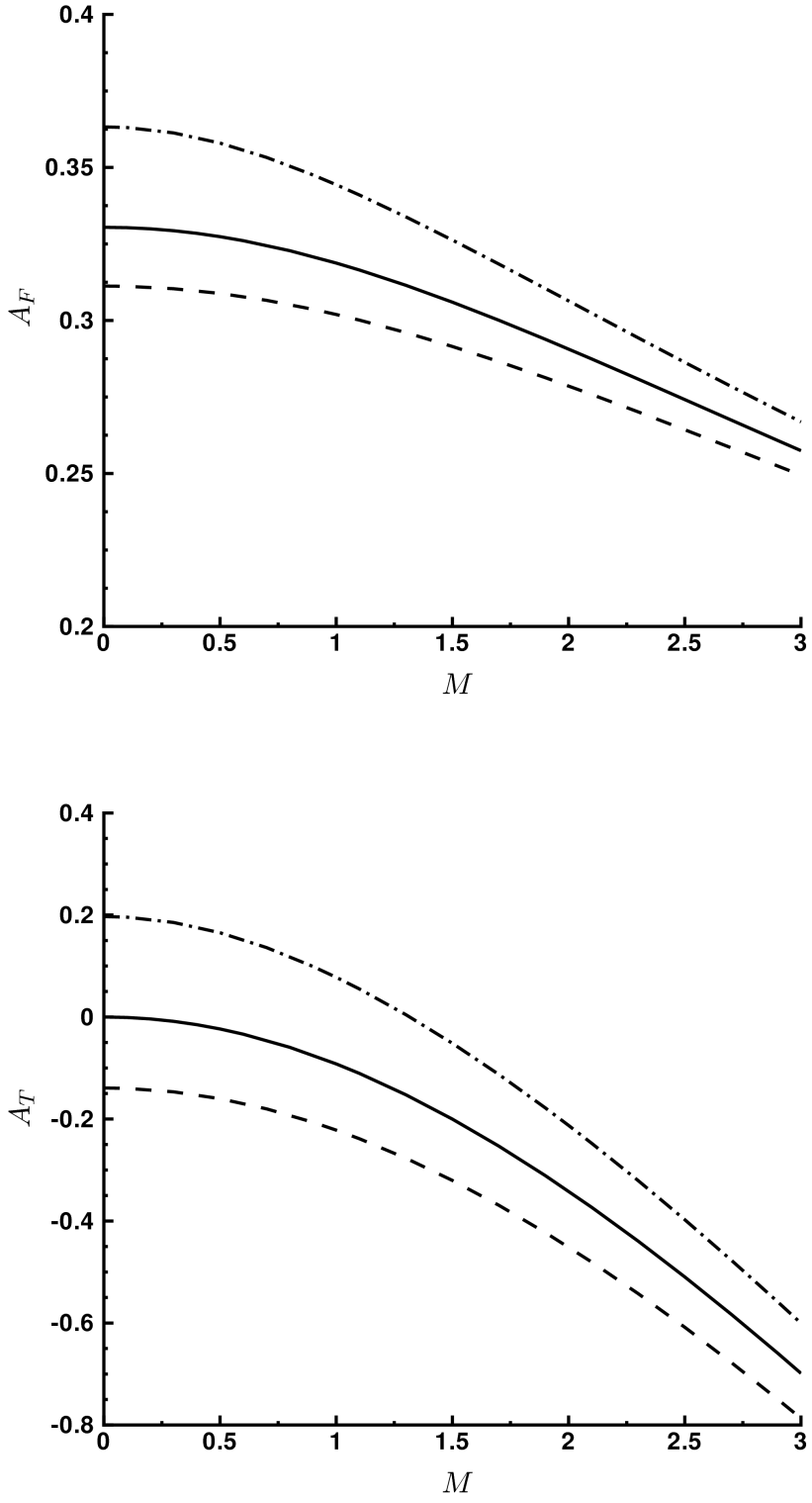


FIG. 18: $A_F$ (top) and $A_T$ (bottom) as functions of Mach number for $T_{dw} = -0.2, 0, 0.2$.

**References**


[1] P. S. Klebanoff. Effect of free-stream turbulence on a laminar boundary layer. *Bull. Am. Phys. Soc.*, 16, 1971.

[2] J. M. Kendall. Boundary layer receptivity to free stream turbulence. *AIAA Paper*, 90-1504, 1990.

[3] K. J. A. Westin, A. V. Boiko, B. G. B. Klingmann, V. V. Kozlov, and P. H. Alfredsson. Experiments in a boundary layer subjected to free stream turbulence. Part 1. Boundary layer structure and receptivity. *J. Fluid Mech.*, 281:193–218, 1994.

[4] M. Matsubara and P. H. Alfredsson. Disturbance growth in boundary layers subjected to free-stream turbulence. *J. Fluid Mech.*, 430:149–168, 2001.

[5] P. J. Schmid and D. S. Henningson. *Stability and Transition in Shear Flows*. Applied Mathematical Sciences, Springer, Vol. 142), 2001.

[6] P. G. Drazin and W. H. Reid. *Hydrodynamic stability*. Cambridge Mathematical Library, 2004.

[7] S. J. Leib, D. W. Wundrow, and M. E. Goldstein. Effect of free-stream turbulence and other vortical disturbances on a laminar boundary layer. *J. Fluid Mech.*, 380:169–203, 1999.

[8] D. W. Wundrow and M. E. Goldstein. Effect on a laminar boundary layer of small-amplitude streamwise vorticity in the upstream flow. *J. Fluid Mech.*, 426:229–262, 2001.

[9] P. Andersson, L. Brandt, A. Bottaro, and D. S. Henningson. On the breakdown of boundary layer streaks. *J. Fluid Mech.*, 428:29–60, 2001.

[10] X. Wu and M. Choudhari. Linear and non-linear instabilities of a Blasius boundary layer perturbed by streamwise vortices. Part 2. Intermittent instability induced by long-wavelength Klebanoff modes. *J. Fluid Mech.*, 483:249–286, 2003.

[11] M.V. Morkovin. Bypass transition to turbulence and research desiderata. *NASA CP-2386 Transition in Turbines*, pages 161–204, 1984.

[12] S. Nagarajan, S. K. Lele, and J. H. Ferziger. Leading-edge effects in bypass transition. *J. Fluid Mech.*, 572:471–504, 2007.

[13] H. L. Dryden. Air flow in the boundary layer near a plate. *NACA Rep.*, 562, 1936.

[14] G. I. Taylor. Some recent developments in the study of turbulence. *Fifth Intl. Congr. for Appl. Mech. (ed. J.P. Den Hartog & Peters)*, pages 294–310, 1939.

[15] D. Arnal and J. C. Juillen. Contribution expérimental a l'etude de la receptivite d'une couche limite laminaire, a la turbulence de l'ecoulement general. *CERT RT 1/5018 AYD - ONERA*, 1978.

[16] J.H.M. Fransson, M. Matsubara, and P. H. Alfredsson. Transition induced by free-stream turbulence. *J. Fluid Mech.*, 527:1–25, 2005.

[17] D. Hernon, E. J. Walsh, and D. M. McEligot. Experimental investigation into the routes to bypass transition and the shear-sheltering phenomenon. *J. Fluid Mech.*, 591:461–479, 2007.

[18] D. Hernon, E. J. Walsh, and D. M. McEligot. Instantaneous fluctuation velocity and skewness distributions upstream of transition onset. *Int. J. Heat Fluid Flow*, 28:1272–1279, 2007.

[19] M. E. Goldstein, S. J. Leib, and S. J. Cowley. Distortion of a flat plate boundary layer by free stream vorticity normal to the plate. *J. Fluid Mech.*, 237:231–260, 1992.

[20] P. Luchini. Reynolds-number-independent instability of the boundary layer over a flat surface: optimal perturbations. *J. Fluid Mech.*, 404:289–309, 2000.

[21] P. Andersson, M. Berggren, and D. S. Henningson. Optimal disturbances and bypass transition in boundary layers. *Phys. Fluids*, 11(1):134–150, 1999.

[22] L. Brandt, P. Schlatter, and D. S. Henningson. Transition in boundary layers subject to free-stream turbulence. *J. Fluid Mech.*, 517:167–198, 2004.

[23] P. Durbin and X. Wu. Transition beneath vortical disturbances. *Annu. Rev. Fluid Mech.*, 39:107–128, 2007.

[24] P. Ricco and X. Wu. Response of a compressible laminar boundary layer to free-stream vortical disturbances. *J. Fluid Mech.*, 587:97–138, 2007.

[25] X. Wu, R. G. Jacobs, J. C. R. Hunt, and P. A. Durbin. Simulation of boundary layer transition induced by periodically passing wakes. *J. Fluid Mech.*, 398:109–153, 1999.

[26] X. Wu and P. A. Durbin. Numerical simulation of heat transfer in a transitional boundary with passing wakes. *Trans. ASME*, 122:248–257, 2000.

[27] N. Kemp. The laminar three-dimensional boundary layer and a study of the flow past a side edge. *MAcs Thesis, Cornell University*, 1951.
[28] T. Cebeci. *Convective Heat Transfer*. Springer-Verlag, 2002.
[29] H. Schlichting and K. Gersten. *Boundary-Layer Theory*. Springer, 2000.
[30] A. N. Gulyaev, V. E. Kozlov, V. R. Kuzenetsov, B. I. Mineev, and A. N. Sekundov. Interaction of a laminar boundary layer with external turbulence. *Izv, Akad. Navk. SSSR Mekh. Zhid. Gaza 6*, pages 700–710, 1989.
[31] P. Ricco. Response of a compressible laminar boundary layer to free-stream turbulence. *PhD Thesis, University of London*, 2006.
[32] P. Graziosi and G.L. Brown. Experiments on stability and transition at Mach 3. *J. Fluid Mech.*, 472:83–124, 2002.
[33] W. O. Criminale, T. L. Jackson, and R. D. Joslin. *Theory and computation in hydrodynamic stability*. Cambridge University Press, 2003.
[34] L. M. Mack. Boundary-layer linear stability theory. *Special Course on Stability and Transition of Laminar flow. AGARD Report 709*, pages 1–81, 1984.
[35] D. W. Dunn and C. C. Lin. On the stability of the laminar boundary layer in a compressible fluid. *J. Aero. Sc.*, 22:455–477, 1955.
[36] S. N. Brown and K. Stewartson. On the propagation of disturbances in a laminar boundary layer. I. *Proc. Camb. Phil. Soc.*, 73:493–503, 1973.
[37] A. Hanifi, P.J. Schmid, and D. S. Henningson. Transient growth in compressible boundary layer flow. *Phys. Fluids*, 8(3):826–837, 1996.
[38] A. Hanifi and D. S. Henningson. The compressible inviscid algebraic instability for streamwise independent disturbances. *Phys. Fluids*, 10(8):1784–1786, 1998.
[39] M. Abramowitz and I. A. Stegun. *Handbook of Mathematical Functions*. Nat. Bureau Stand. Appl. Math. Ser. 55, 1964.
[40] S. H. Lam and N. Rott. Theory of linearized time-dependent boundary layers. *Cornell University Grad. School of Aero. Engineering Dept. - AFOSR TN-60-1100*, 1960.
[41] S. H. Lam and N. Rott. Eigen-Functions of linearized unsteady boundary layer equations. *J. Fluids Eng.*, 115:597–602, 1993.
[42] M. E. Goldstein. The evolution of Tollmein-Schlichting waves near a leading edge. *J. Fluid Mech.*, 127:59–81, 1983.
[43] L. M. Mack. Linear stability theory and the problem of supersonic boundary-layer transition. *AIAA J.*, 13(3):278–289, 1975.
[44] E. Reshotko. Drag reduction by cooling in hydrogen-fueled aircraft. *J. Aircraft*, 16:584–590, 1979.
[45] M. R. Malik. Prediction and control of transition in supersonic and hypersonic boundary layers. *AIAA J.*, 27(11):1487–1493, 1989.
[46] J. A. Masad and A. H. Nayfeh. Effect of heat transfer on the subharmonic instability of compressible boundary layers. *Phys. Fluids*, 3(9):21482–163, 1991.
[47] V. I. Lysenko and A. A. Maslov. Transition reversal and one of its causes. *AIAA J.*, 19(6):705–708, 1981.
[48] V. I. Lysenko and A. A. Maslov. The effect of cooling on supersonic boundary-layer stability. *J. Fluid Mech.*, 147:39–52, 1984.
[49] F. T. Smith. On the first-mode instability in subsonic, supersonic or hypersonic boundary layers. *J. Fluid Mech.*, 198:127–153, 1989.
[50] X. Wu. Generation of Tollmien-Schlichting waves by convecting gusts interacting with sound. *J. Fluid Mech.*, 397:285–316, 1999.
[51] The notation $M = 0$ indicates $M^2 \ll 1$, so that the viscous heating effects due to the square of the velocity gradients are negligible. In this case, the density changes may only be due to the wall heat transfer, and the flow can be therefore assumed incompressible for adiabatic wall conditions.

**List of Figures**

FIG. 1: Schematic of the physical domain.

FIG. 2: Maximum (across $\eta$) of the streamwise velocity (top) and temperature fluctuation (bottom) for $M$=2, $T_{dw} = 0.2$ and $\kappa_z = 0$. In this figure and in figure 3, the lines represent cases with $\overline{\tau}(0) = 0$ and the symbols denote cases with $\partial\overline{\tau}/\partial\eta|_{\eta=0} = 0$.

FIG. 3: Maximum (across $\eta$) of the streamwise velocity (top) and temperature fluctuation (bottom) for $M$=2, $T_{dw} = 0.2$ and $\kappa_z = 1$.

FIG. 4: Maximum (along $\eta$) of velocity (top) and temperature (bottom) fluctuations for different Mach numbers, adiabatic-wall conditions and $\kappa_z = 0$.

FIG. 5: Maximum (along $\eta$) of streamwise velocity (top), temperature (middle) and mass-flux fluctuations (bottom) for $M$=0.75 (left), $M$=2 (right) and $\kappa_z = 0$.

FIG. 6: Streamwise velocity (top), temperature (middle) and spanwise (bottom) velocity fluctuations for $M$=2 at $\overline{x} = 2$ for $\kappa_z = 0$. The black circles indicate the solution obtained by the Neumann wall boundary condition on $\overline{\tau}$ (every four data point is plotted).

FIG. 7: Maximum (along $\eta$) of temperature fluctuations at $\overline{x}$=1 for $\kappa_z = 0$ as a function of $T_{dw}$ for different Mach numbers (see legend in graph).

FIG. 8: Wall-normal position $\eta$ of the streamwise velocity maximum for $M$=0.75 (top), $M$=2 (bottom) and $\kappa_z = 0$.

FIG. 9: Spanwise velocity fluctuations at $\overline{x} = 80$ for $\kappa_z = 0$ for $M = 0$ (top) and $M = 2$ (bottom). The circles indicate the edge-layer solutions and the lines represent the boundary-region solutions.

FIG. 10: Maximum (along $\eta$) of streamwise velocity (top-left), temperature (middle-left) and mass-flux fluctuations (bottom-left) as functions of $\overline{x}$ for $M = 2$ and $\kappa_z = 1$. The thick-line graphs on the right present the difference between the heat-flux curves (denoted by subscript $ht$) and the adiabatic-wall curves (indicated by subscript $ad$).

FIG. 11: Streamwise velocity (top), temperature (middle) and spanwise velocity (bottom) for $M = 2$ at $\overline{x} = 2$ for $\kappa_z = 1$. The black circles indicate the solution obtained by the Neumann wall boundary condition on $\overline{\tau}$ (every four data point is plotted).

FIG. 12: Streamwise velocity $|\tilde{u}|_{max} = \kappa_z^2|\overline{u}|_{max}$ as a function of $\tilde{x} = \kappa_z^2\overline{x}$ for wall-heating ($T_{dw} = -0.2, H$), adiabatic-wall ($T_{dw} = 0, A$), and wall-cooling conditions ($T_{dw} = 0.2, C$) at $M = 0$. Results for $\kappa_z = 2, 3, 4$ are shown.

FIG. 13: Maximum of streamwise velocity component as a function of $\overline{x}$ for $\kappa_z = 0.02$ and $M = 0.8$ (top) and $M = 3$ (bottom) for $T_{dw} = -0.2, 0, 0.2$.

FIG. 14: Real part of streamwise velocity component $\overline{u}$ at $\eta = 2$ as a function of $\overline{x}$ for $M = 3$, $\kappa_z = 0.02$ for wall cooling ($T_{dw} = 0.2$ - top), adiabatic wall ($T_{dw} = 0$ - middle) and wall heating ($T_{dw} = -0.2$ - bottom).

FIG. 15: Comparison of the wavenumber (top) and growth rate (bottom) of the growing disturbances for $M = 3$ and $\kappa_z = 0.0005$. The thin lines indicate the boundary-region solutions and the thick lines denote the triple-deck solutions. Wall heat-transfer conditions are for $T_{dw} = -0.2, 0, 0.2$. The black dots indicate the growth rates and starting location of the instability.

FIG. 16: Schematic of the flow regimes and the wall heat transfer effects on the streamwise velocity fluctuations for constant $\lambda_x^*$, $M = \mathcal{O}(1)$ and $\kappa_z = \kappa_y$.

FIG. 17: $\beta_c$ as function of Mach number for $T_{dw} = -0.2, 0, 0.2$.

FIG. 18: $A_F$ (top) and $A_T$ (bottom) as functions of Mach number for $T_{dw} = -0.2, 0, 0.2$.